International Journal of Biological Macromolecules xxx (xxxx) 125572

Contents lists available at ScienceDirect

International Journal of Biological Macromolecules

journal homepage: www.elsevier.com/locate/ijbiomac

Potential of curcumin and niacin-loaded targeted chitosan coated liposomes to activate autophagy in hepatocellular carcinoma cells: An in vitro evaluation in HePG2 cell line

Nemany A.N. Hanafy [a,*], Rehab Fouad Sheashaa [b], Eman A. Moussa [b], Magdy E. Mahfouz [b]

[a] Institute of Nanoscience and Nanotechnology, Kafrelsheikh University, 33516 Kafrelsheikh, Egypt
[b] Department of Zoology, Faculty of Science, Kafrelsheikh University, 33516 Kafrelsheikh, Egypt

ARTICLE INFO

Keywords:
Niacin
Curcumin
Autophagy
Nanoparticles
Liposomes
Chitosan

ABSTRACT

The objective of this study is to activate autophagy in hepatocellular carcinoma for the enhancement of its cellular degradation. Liposomes incorporated chitosan in the core used to improve the stability of lecithin and increase the niacin loading efficiency. Additionally, curcumin as a hydrophobic molecule entrapped into liposomal layers and used as a face layer to minimize the release of niacin in physiological pH 7.4. Folic acid-conjugated chitosan was used to facilitate the delivery of liposomes into a specific location of cancer cells. TEM, UV Visible spectrophotometer, and FTIR confirmed the successful liposomal formation and good encapsulation efficiency. Based on the cellular proliferation of HePG2, the results revealed that there was a significant inhibition of growth rate of HePG2 after 48 h of incubation at a concentration of 100 μg/mL by 91 % ± 1 %, $P \leq 0.002$ (pure niacin), 55 % ± 3 %, $P \leq 0.001$ (pure curcumin), 83 % ± 1.5 %, $P \leq 0.001$ (niacin NPs), and 51 % ± 1.5 % $P \leq 0.0001$ (curcumin-niacin NPs) of relative to the control. Increasingly, The expression of mRNA of mTOR was significantly increased by 0.72 ± 0.08 $P \leq 0.001$, 1 ± 0.1, 0. $P \leq 0.001$, 5 ± 0.07 $P \leq 0.01$, and 1.3 ± 0.02 $P \leq 0.001$ *folds)* in pure niacin, pure curcumin, niacin NPs and curcumin -niacin NPs, respectively, relative to the control with an expression of 0.3 ± 0.08. Additionally, the expression of p62 mRNA was significantly increased by 0.92 ± 0.07 $P \leq 0.05$, 1.7 ± 0.07 $P \leq 0.0001$, 0.72 ± 0.08 $P \leq 0.5$, and 2.1 ± 0.1 $P \leq 0.0001$ *folds* relative to that of the control with an expression of 0.72 ± 0.08. The results highlight the efficient therapies of biomaterials derived from natural sources that can be used in cancer therapies instead of traditional chemotherapies.

1. Introduction

Hepatocellular carcinoma (HCC) is the most invasive cancer cell type among many cancer cells because of its strong angio-invasive potential and drug resistance [1]. HCC has the highest incidence of specific cancer cases in Egypt. In 2020, HCC had an estimated incidence of 20 % (27,895 cases) among 134,632 cancer cases [2]. Doxorubicin, irinotecan, gemcitabine, 5-fluorouracil, and sorafenib have been used to treat HCCs. However, HCCs are chemotherapeutic resistant because of their high expression of the P-glycoprotein gene product, dihydropyrimidine dehydrogenase, and the multidrug resistance gene, MDR-1 [3]. Autophagy is an intracellular process that facilitates the degradation of dysfunctional cytoplasmic components using endogenous lysosomes [4]. Under abnormal conditions such as hypoxia, cell starvation, and lack of growth factors, autophagy can be activated, resulting in the degradation of intracellular contents [5,6]. It reported that niacin can increase the NAD+/NADH ratio inducing therapeutic normalization of NAD+/NADH balance through autophagy. This process has provided new insights into activating autophagy in human breast adenocarcinoma cells, ovarian, pancreatic, and prostate cancer cells [7]. Our hypothesis aimed to activate autophagy in the HePG2 cell line using a combination of niacin and curcumin loaded targeted chitosan liposomal formulation. Chitosan is used widely in biomedical applications because of its biodegradability, good biocompatibility, and non-toxic properties. Therefore, chitosan can improve mucoadhesive properties and anticancer drug efficiency [8]. Folic acid (FA), one of the most common ligands, can be attached to a high-affinity binding receptor. Therefore, folate receptors are highly expressed in several human cancers [9–12]. In the current study, niacin and curcumin as natural compounds were inserted onto liposomal layers formed by 3-sn-

* Corresponding author.
E-mail address: nemany.hanafy@nano.kfs.edu.eg (N.A.N. Hanafy).

https://doi.org/10.1016/j.ijbiomac.2023.125572
Received 29 November 2022; Received in revised form 18 June 2023; Accepted 24 June 2023
0141-8130/

phosphatidylcholine of soy lecithin and cholesterol. Lecithin vesicles were prepared by the thin film hydration method as described previously and summarized in Table 1 [13,15–27]. In literature reports, 2,2-Diphenyl-1-picrylhydrazyl (DPPH) was used to improve the stability of lipid layers [18]. However, lecithin is still an attractive natural material due to its wide availability, low cost, and it's safe for pharmaceutical applications [27]. To improve the liposomal structure, chitosan was incorporated into the inner face of liposomal layers allowing lecithin as a negatively charged mixture of phospholipids to be attached strongly with the positively charged amino group of chitosan.

2. Materials and methods

2.1. Chemical reagents

Cholesterol was obtained from LANXESS, Germany; Soy lecithin and chitosan from Sigma-Aldrich Inc., nicotinic acid from Central drug house, FA from LOBAL Chemie, and curcumin LR from SDFCL. Chitosan, acridine orange, ethidium bromide, ethanol, and chloroform were purchased from Sigma Company, Egypt.

2.2. Fabrication of free liposome, niacin NPs, and CUR-niacin NPs

Liposomes were prepared by the thin film hydration method described by [13]. Curcumin and other drugs were added separately during fabrication as described by [18,23] with modification. Briefly, a mass of 20 mg of soy lecithin was dissolved in 0.5 mL chloroform and mixed with 14 mL of absolute ethanol with stirring for 10 min at 70 °C. After that, 100 mg of niacin dissolved in 2 mL of 1 N NaOH was added slowly into 2 mL of chitosan (5 mg/20 mL) under continuous stirring for 10 min. The niacin-chitosan solution was added to soy lecithin. Additionally, a volume of 35 mL of cholesterol dissolved in 0.5 mL chloroform was added and the mixture was continuously stirred for a further 20 min. The solvent was removed by the rotary evaporators at 70 °C and then the hydration process was carried out with 10 mL of phosphate buffer saline (pH 7.2). For functionalization, 5 mg folic acid dissolved by 20 μL NaOH(1 N) was mixed in a brown bottle under a stirrer with 0.25 mg/1 mL chitosan for 3 h. After that, the mixture was dialyzed against distilled water for 24 h with water removal each 6 h. The mixture was further lyophilized and stored. 14 mL of folic acid-conjugated chitosan was added to the mixture before stirring for another 20 min. The formed nanoparticles were dialyzed against distilled water for 24 h before they were stored at −20 °C for lyophilization. The resultant nanoparticles were freeze-dried on Martin Christ lyophilizer at −58 °C and 0.3 mbar for 72 h.

2.3. Characterization

The encapsulating niacin NPs and curcumin-niacin NPs were characterized by using Scanning Electron Microscope (SEM), Fourier Transform Infrared Spectroscopy (FTIR), Zeta Potential, and UV–Vis spectroscopy.

2.3.1. Scanning electron microscopy (SEM)

For SEM analysis, lyophilized niacin NPs and curcumin-niacin NPs were put onto a template of SEM. Samples were sputtered with a 5 nm gold layer and measurements were conducted under 5 kV-accelerating potential electron beam by using SEM (JEOL, JSM–IT 100). Images were processed by using the software SEM/JSM 5000.

Table 1
Describes the previous published reports on liposomal formulations, their methods and chemical used in fabrication.

	Methods	Chemicals	Result	Refs
Naeem et al., 2015	Thin film hydration method	Lecithin (phosphatidylcholine) from soybean	Good dispersion and high stability	[13]
Cheng, et al., 2017	pH-driven method, the thin film method, and the ethanol injection method.	Phospholipid [Lipoid S75, consisting mainly of phosphatidylcholine (70 %), phosphatidylethanolamine (10 %) and lysophosphatidylcholine (2 %)]	The CLs prepared by the thin film method displayed high bioaccessibility but poor storage stability, and those prepared by the ethanol injection method were stable during storage but showed low bioaccessibility.	[14]
Li et al., 2018	Thin film evaporation.	Phospholipid, cholesterol, pluronic and curcumin	Showed sustained release.improved thermal and pH stability. Increased bioaccessibility.	[15]
He et al., 2018	Thin-film evaporation method	Cholesterol (CH) and soybean phosphatidylcholine, Thiamine (TH) and niacin (NA), stearamine	Sustained, mild hypoglycemic effect	[16]
De Leo et al., 2018	Micelle-to-vesicle transition	Ethanol, Sephadex G-50 medium, cholesterol, curcumin, oleic acid,	very stable, showing a low tendency to aggregate both at 4 °C and 25 °C.	[17]
Huang, et al., 2019	Thin-film evaporation method	Egg yolk phosphatidylcholine, 2,2-Diphenyl-1-picrylhydrazyl (DPPH), Tween 80, Curcumin and resveratrol	Exhibited high encapsulation efficiency, and improved stability for these beneficial compounds.	[18]
Schmitt et al., 2020	Thin-film evaporation method	Cholesterol, dipalmitoylphosphatidylcholine, curcumin	Sustained drug release at physiological pH	[19]
Wei et al., 2020	Thin film hydration	Curcumin (CURC) Phospholipids (soybean lecithin for injection use, with phosphatidylcholine content >70 %) Cholesterol	liposomal CURC is still more stable in an acidic external environment	[20]
López-Machado et al., 2021	Thin-film hydration method	Egg yolk phosphatidylcholine (PC) and cholesterol, polysorbate 80and curcumin	Better skin deposition of liposomal curcumin	[21]
Estephan et al., 2021	Solvent evaporation method	Curcumin, chitosan and diarachidonyl phosphatidyl choline	Chitosan changes membrane permeability of liposomes	[22]
Song et al., 2022	Thin–film hydration method	Soybean lecithin, cholesterol, DP, curcumin, Tetrandrine	Liposomes can improve the solubility of CUR and Tetrandrine, break the restrictions on their clinical application due to their chemical properties and increase anticancer activity	[23]
Quach et al., 2022	Thin-film method	Curcumin, soy lecithin, ginger oil, cholesterol and tween 80	The addition of ginger oil in the lipid phase with lecithin allowed the formation of functional lipid nanoparticles	[24]
Othman et al., 2022	Thin film hydration method	Curcumin, 1,2-dimyristoyl-*sn-glycero*-3-phosphocholine	study suggests that by applying different layers on the liposome surface, the drug release and anti-cancer activity of curcumin can be enhanced	[25]
De Leo V et al., 2023	Thin-film evaporation method	1,2-distearoyl-sn-glycero-3-phosphoethanolamine-N-[amino (polyethylene glycol)-2000] Cholesterol	Increase the oral bioavailability of both Curcumin and Hydroxytyrosol	[26]

2.3.2. Zeta potential and DLS measurements

The electrophoretic mobility of samples was determined by photon correlation spectroscopy (Brookhaven) by using a Zeta Nano Sizer. All measurements were performed at 25 °C. The following five successful running measurements were taken for analysis.

2.3.3. UV–vis spectroscopy

The absorbance of samples was measured using a JASCO V-770 UV Visible Absorbance Spectrophotometer. 500 μl of the fabricated assembly was diluted into 4 mL with distilled water and then scanned at 200–800 nm. The data were analyzed by the Origin 8 program (https://www.originlab.com/).

2.3.4. Fourier transform infrared spectroscopy (FTIR)

FTIR experiments were carried out by a JASCO Fourier Transform Infrared Spectrometer (JASCO, JAPAN, model no. AUP1200343) used to identify the structure of individual molecules and the composition of molecular mixtures in the range of 400–4000 cm^{-1} using the KBr pellet method. For all the tests, at least three scans per sample were recorded on different regions, and representative spectra were analyzed.

2.4. Determination of encapsulation efficiency and in vitro drug release study

After centrifugation of encapsulated NPs, the supernatant was used to measure the loading capacity of the loading niacin and curcumin using a UV–visible spectrophotometer. Therefore, the pure niacin and curcumin were subjected to spectrophotometric analysis at 270 nm. The concentrations of niacin and curcumin were determined separately following their known serial concentrations at 10 μg to 60 μg (R^2 = 0.9967). The encapsulation efficiency (%) was calculated using the following equation according to [20].

Encapsulation efficiency of Niacin (%)
= Conc. of total niacin
− Conc. of free niacin (supernatant)
\Conc. of total niacin × 100.
Encapsulation efficiency of CUR (%)
= Conc. of total CUR
− Conc. of free CUR (supernatant)
\Conc. of total CUR × 100.
The total encapsulation efficiency (%)
= The amount of CUR
/Niacin encapsulated within liposomes
/Total amount of CUR/Niacin added × 100

The in vitro release study was used to investigate the continuous drug release with time in Phosphate Buffer Saline (PBS) (pH 7.4, representing the physiological environment) and PBS (pH 6.5, representing the cancer environment) according to the method of Hanafy et al. [11,12].

Briefly, 16 mg each of pure niacin, pure curcumin, niacin NPs, and curcumin-niacin NPs were suspended in 10 mL PBS and transferred into dialysis bags (molecular weight 12,000–14,000 Da). They were immersed in a 40 mL release medium at 37 °C with continuous stirring at 100 rpm. After each incubating time, 3 mL was aspirated from each baker to determine the quantity of niacin and curcumin released after 0,1,2,3,4,5,6,24,48,and72 h. The baker's solution was replaced after every aspiration with the same volume of freshly prepared release medium containing 1 % Tween 80 for > 50 h. The absorbance of niacin and curcumin was measured using a UV–Vis spectrophotometer at a wavelength of 270 nm.

The percentage of cumulative drug release was measured using the constructed standard calibration curve. The mean release of three measurements was used to evaluate the drug release for each point.

Concentration of drug (μg/mL)
= (slope × absorbance) ± intercept
Amount of drug
= Concentration × Dissolution bath volume
× Dilution factor released mg/mL 1000.
Cumulative percentage
= Volume of sample withdrawn (ml)
× P (t–1) + Pt release (%) Bath volume.

where Pt = Percentage release at time t, e P (t – 1) = Percentage release prior to't'.

2.5. Characterization of FA

FA conjugated chitosan was characterized by using FTIR, and UV visible spectrophotometer. Additionally, the concentration of FA-attached liposomes was measured by using a UV–Vis spectrophotometer. Firstly, the calibration curve of standard FA in 1 mg/mL NaOH was prepared with a concentration range of 25–150 μg/mL (y = 0.0225× + 0.1085; R^2 = 0.9939). After the encapsulation process, the supernatant was used to detect the loading capacity of the FA conjugation using the following equations: The concentration of non-conjugated FA (supernatant) (μg/mL) = (slope × absorbance) ± intercept.

Encapsulation efficiency of FA (%)
= Conc.of total FA
− Conc.of free FA (supernatant) \Conc.of total FA
× 100.

2.6. Stability of nanoparticles in different media

Stability of niacin NPs and CUR -niacin NPs was investigated in different media (distilled water, saline, and DMEM cell culture medium with 5 % FBS) by measuring their hydrodynamic diameter and polydispersity index (PDI) after their incubation for 1 day and 5 days. The result was taken by Brookhaven at 25 °C. Each measurement was performed using at least three sets of 10 runs.

2.7. In vitro assays

2.7.1. Cytotoxicity (MTT) assay

To assess the effect of curcumin, niacin, niacin NPs, and curcumin-niacin NPs on HePG2 tumor cell growth, cell viability was evaluated by the 3-(4,5-dimethylthiazol-2-yl)-2,5 diphenyl-tetrazolium-bromide (MTT; Sigma-Aldrich Inc., St. Louis, MO, USA) assay. Briefly, after drug exposure, 5 mg/mL of MTT was added to each well and the reaction was allowed to proceed for 3–4 h at 37 °C. The culture medium was then removed and precipitated formazan crystals were dissolved by adding 200 μL DMSO. The absorbance of each well was measured at 570 nm and directly correlated to the number of remaining viable cells. Absorbance data were normalized to the percentage of control cells and then they were graphed [28].

2.7.2. Autophagy assay by using flow cytometry

Autophagic cell death was assayed using acridine orange lysosomal stain coupled with flow cytometric analysis. After the cells were treated with test compounds for 24 or 48 or 72 h and chloroquine (10 μM) for 24 or 48 or72 h as a positive control, 10^5 cells were collected by trypsinization and washed twice with ice-cold PBS (pH 7.4). Cells were stained with acridine orange (10 μM) and incubated in the dark at 37 °C for 30 min. After they were stained, cells were injected into a ACEA Novocyte™ flowcytometer (ACEA Biosciences Inc., San Diego, CA, USA) and acridine orange fluorescent signals were analyzed using FL1 signal detector (λex/em 488/530 nm). For each sample, 12,000 events

were acquired and net fluorescent intensities (NFI) were quantified using the ACEA NovoExpress™ software (ACEA Biosciences Inc., San Diego, CA, USA). The NFI were detected in two directions, namely, the forward scatter (FSC), which is proportional to cell size and the side scatter, which is proportional to cell granularity [29]. The data were analyzed by Image J program https://imagej.nih.gov/ij/download.html.

2.7.3. Evaluation of gene expression using RT-PCR

Total ribonucleic acid (RNA) was extracted by the Trizol reagent (Invitrogen, Carlsbad, CA) following the manufacturer's protocol [30]. Complementary DNA (cDNA) was synthesized from RNA using a first-strand cDNA synthesis kit (Fermentas, Vilnius, Lithuania), following the manufacturer's protocol. The thermocycler for cDNA synthesis was set up at 37 °C for 30 min. Quick PCR (qPCR) was performed using an Applied Biosystems 7300 Real Time PCR System (Applied Biosystems, Branchburg, NJ, USA) at three conditions, 95 °C for 5 min, 45 cycles at 95 °C for 30 s, and 60 °C for 1 min. The Expression levels of mRNA were normalized to the GAPDH gene as endogenous control. The relative differences between the control and treatment groups were determined. Primers and probes for the qPCR were designed using Allele ID 6. All primers are listed in Table 2.

2.8. Cancer bio-image

HePG2 cells were seeded into 24 multiwell microplates (10^4 cells/well). The cells were grown in 500 μL DMEM High Glucose (4,5 g/l) supplemented with 5 % L-Glutamine, 10 % fetal bovine serum, and 5 % penicillin/streptomycin in a humidified atmosphere with 5 % CO_2 at 37 °C. After 24 h, 50 μg pure niacin, niacin NPs, pure curcumin, curcumin-niacin NPs were added to each well separately and incubated in a humidified atmosphere of 37 °C, 5 % CO_2. HepG2 cells were fixed with 4 % paraformaldehyde before washing with PBS, pH 7.2. Cells were stained separately using different dyes such as AO/EB, PI, and DAPI (nuclear stain) for 30 min and then washed twice. Images were captured by fluorescence microscopy [31].

3. Results

3.1. Characterization

Chitosan can increase cellular penetration due to its ability to open the tight junctions of the epithelial cells. Hence, it facilitates both the paracellular and transcellular transport of drugs. In the small intestine, chitosan can adhere to the mucus layer forming a complex through ionic or hydrogen bonding as well as through hydrophobic interactions [32]. A literature review reveals the advantages of liposomes coated by chitosan in protecting their layers and facilitating their cellular penetration [22]. To improve liposome stability, chitosan was incorporated into the inner core of liposomal layers by mixing it with lecithin during fabrication. In previous work, Ginger Oil was mixed with Lecithin during fabrication to increase the stability of the liposomal layers [24]. For the first time, chitosan alone or chitosan attached niacin was inserted into the inner core of liposomes allowing lecithin as a negatively charged mixture of phospholipids to be attached strongly with the positively charged amino group of chitosan. This strategy might increase the loading capacity of niacin and improve liposomal structure. Additionally, chitosan-conjugated folic acid is used to coat the liposomal formulation as well. Chitosan-coated liposomes were assembled into a 3D structure (Fig. 1; A–C) & Scheme 1). Since the TEM image observed the morphological appearance of niacin NPs and CUR-niacin NPs as a spherical shape.

Zeta potential represents a measure of system stability based on net charge and systemic attraction or repulsion of developed NPs [33]. In the current study, free liposomes, niacin NPs, and curcumin-niacin NPs exhibited zeta potentials of −39 mV, −15 mV, and − 42 mV, respectively. The results indicate that NPs had good stability and high assembly. Additionally, curcumin-loaded niacin NPs improved the assembled structure of niacin NPs providing clear interaction between moieties of structure. The polydispersity index (PDI), used as an indicator of the size distribution of NP systems, displayed narrow particle size distributions of 0.325, 0.359, and 0.379, respectively, for the three NP formulations. The difference between the PDI of free liposomes and niacin NPs was 0.034, and that between niacin NPs and curcumin-niacin NPs was 0.02 (Fig. 1; D).

The size of nanoparticles measured by dynamic light scattering was 567 nm, 261 nm, 100 nm, 160 nm, and 240 nm for free liposomes, free niacin, niacin NPs, free curcumin, and CUR-niacin NPs, respectively (Fig. 1; E).

UV visible spectrophotometer showed the main characteristic absorption of free niacin at approximately 210 and 260 nm. Whereas niacin-loaded liposomes exhibited a peak at 220 nm and overlayed peak with FA at 280 nm, curcumin-niacin NPs showed abroad peak between 326 and 389 nm related to overlayed absorption of curcumin and FA (Fig. 1; F) [34].

FTIR is an effective analytical method used for detecting functional chemical groups and characterizing covalent bonding information. In the current study, the FTIR spectrum of cholesterol showed a broad band at 3432 cm^{-1} indicating a stretching vibration of OH. The symmetric and anti-symmetric stretching vibrations in CH2 groups of alkyl chains were measured at 2989 cm^{-1} and 2882 cm^{-1}, respectively. A strong band detected at 1716 cm^{-1} was attributed to the double bond in the second ring of the cholesterol structure [35].

Similarly, the soy lecithin spectrum showed a broad and intense band at 3400 cm^{-1} that was attributed to OH stretching. A strong band detected at 1743 cm^{-1} was attributed to stretching vibrations of the carbonyl ester bond. Phosphate groups were detected at 1220 cm^{-1} and 1032 cm^{-1} as anti-symmetric and symmetric modes (Fig. 2; A).

In the chitosan spectrum, FTIR showed NH and OH stretching vibrations mostly at 3432 cm^{-1}. The absorption bands at 2869 cm^{-1} were attributed to C—H symmetric and asymmetric stretching, respectively. The presence of residual *N*-acetyl groups was confirmed by the bands at 1623 cm^{-1} (C═O stretching of amide I) and the small band at 1582 cm − 1 that corresponds to N—H bending of amide II. While 1349 cm^{-1} band assigned to (C—N stretching of amide III), respectively (Fig. 2; A).

A spectrum of folic acid alone showed a band at 1702 cm^{-1} that was assigned to the carboxyl group of FA [36]. In the spectrum of folic acid-conjugated chitosan, the chitosan amide I band was detected at 1623 cm^{-1} and the amide II band at 1555 cm^{-1}. While the band located at 1729 cm-1 was considered for carboxyl amide bond interaction.

The main characteristic peaks of folic acid-conjugated chitosan were detected in the spectrum of free liposomes at 1729 cm^{-1} and 1623 cm^{-1} for carboxyl amide bond interaction [37].

In Fig. 2, the spectrum of free niacin showed stretching vibration of C═O (COO) at 1716 cm − 1. There was a broad band at 2440 cm − 1 that was attributed to C═N of the pyridine ring [38]. In niacin NPs, the FTIR spectrum showed main characteristic peaks of folic acid-conjugated chitosan at 1729 cm^{-1} and 1623 cm^{-1} as main peaks for carboxylic amino interaction. Curcumin showed its signature peaks at 3500 cm^{-1} (phenolic O—H stretching vibration), 1628 cm^{-1} (aromatic

Table 2
Forward and reverse primers of the selected genes.

Gene name	Forward primer (5′-3′)	Reverse primer (5′-3′)
Atg7	CAGTTTGCCCCTTTTAGTAGTGC	CCAGCCGATACTCGTTCAGC
p62	GCACCCCAATGTGATCTGC	CGCTACACAAGTCGTAGTCTGG
mTOR	ATTCAGATCGCTGGCAGCCT	CCCTGTGTTCAGCACCTCCA
Beclin1	CCATGCAGGTGAGCTTCGT	GAATCTGCGAGAGACACCATC
GAPDH	GGTGAAGGTCGGAGTCAAC	AGAGTTAAAAGCAGCCCTGGTG

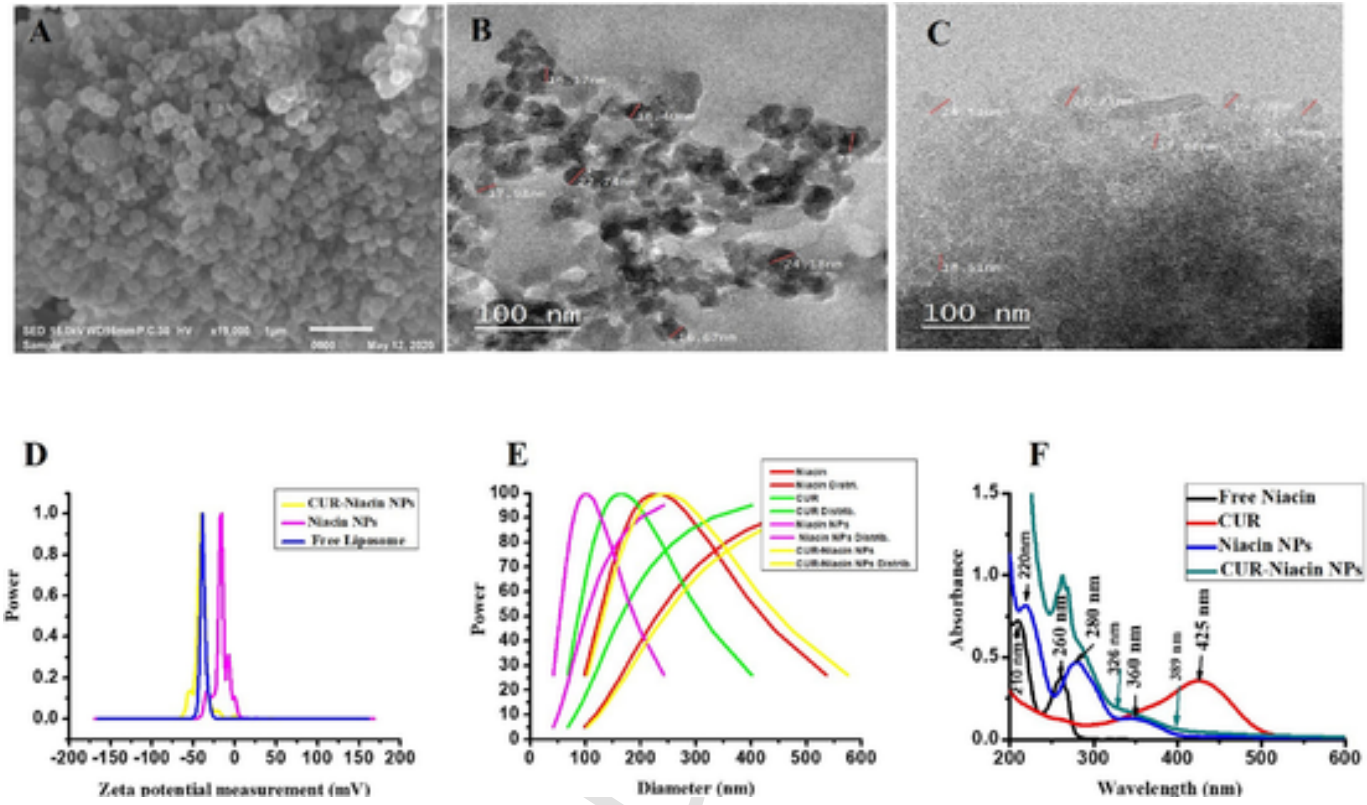

Fig. 1. Characterization of the liposome NPs, niacin NPs, and curcumin(CUR)-niacin NPs. A: SEM images of pure niacin. B: TEM images of niacin NPs. C: TEM images of CUR-niacin NPs. D: Zeta potential measurement. E: Nanosizer and quality of NPs distribution of pure niacin, niacin NPs, CUR-niacin NPs. F: UV visible spectrophotometer of pure niacin, pure CUR, niacin NPs, and CUR-niacin NPs.

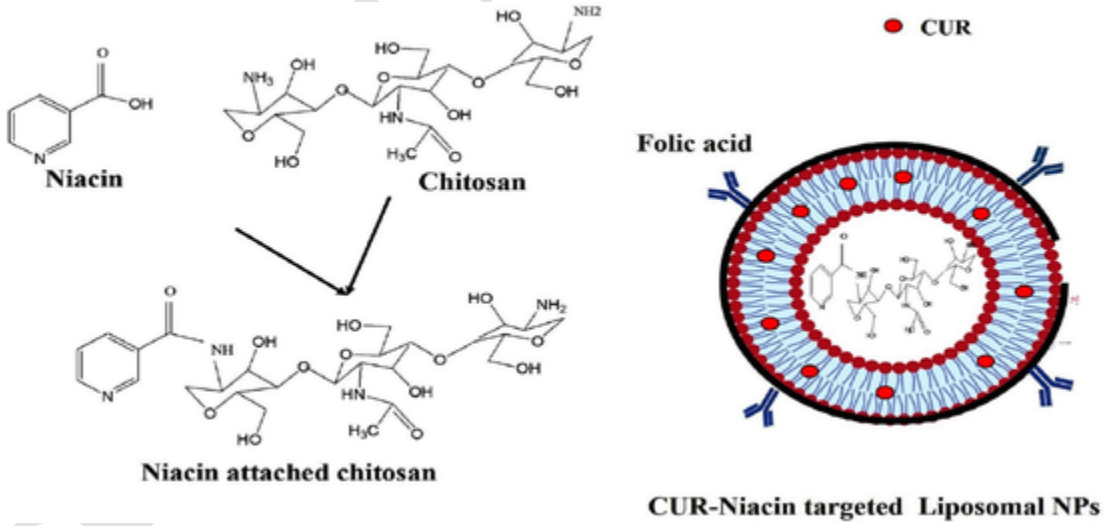

Scheme 1. Illustrates chemical structure of niacin attached chitosan and loaded liposomal targeted therapy.

moiety C═C stretching), and 1501 cm^{-1} (C═O and C═C vibrations). The FTIR spectrum of curcumin -niacin NPs showed a broad band at 3405 cm^{-1} that was attributed to the stretching vibration of phenolic OH. The band at 1623 cm^{-1} was shifted to 1648 cm^{-1} and the band at 1541 cm^{-1} was shifted to 1557 cm^{-1} after curcumin interaction compared to niacin NPs (Fig. 2; B).

The result confirms the successful formulation of liposomal structure and it is in agreement with results obtained by zeta potential and UV visible spectrophotometer.

In the current study, the amount of FA-conjugated NPs was calculated from a standard curve of 1 mg/mL pure FA (R2 = 0.9939). After encapsulation process, the supernatant was collected by centrifugation, and the concentration of non-conjugated FA was estimated. The percentage of encapsulation efficiency of FA was detected as 87 ± 0.42 % (Fig. 3; A–C). The result showed significant conjugation of FA with chitosan-coated liposomes because of the amino contents of chitosan and the good carboxylic activation of FA.

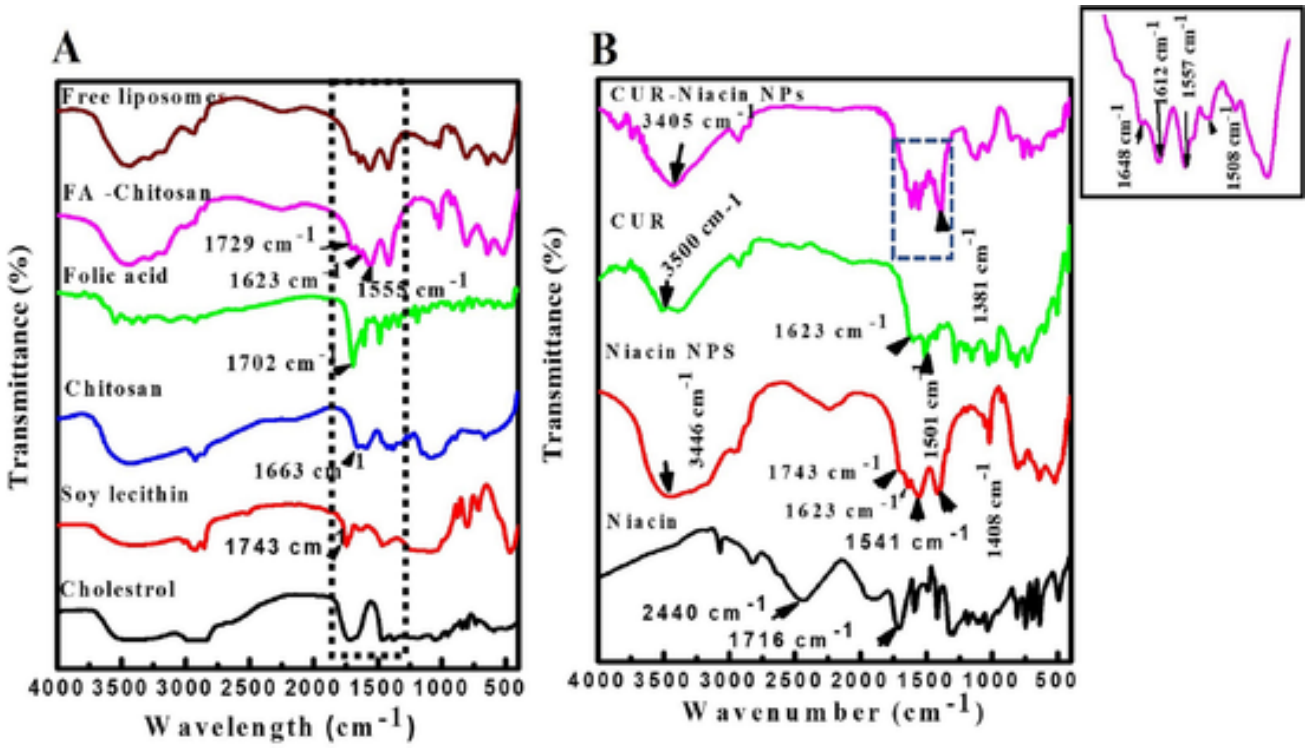

Fig. 2. The FTIR spectra of A: Cholesterol, Phospholipid, Chitosan, Folic acid, FA-Chitosan, and Free liposomes. B: Niacin, Niacin NPs, curcumin, and CUR-Niacin NPs.

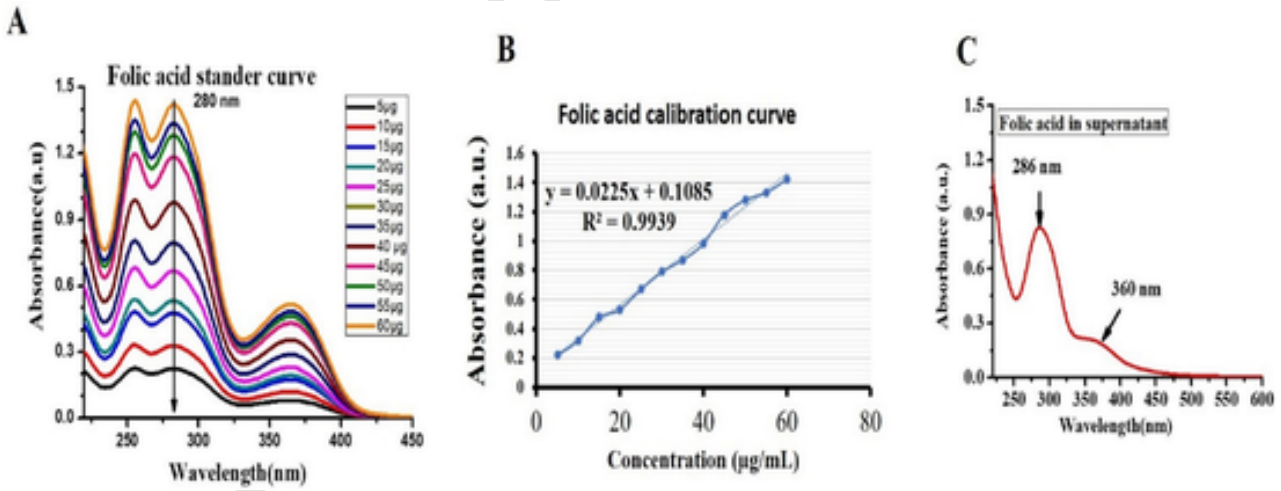

Fig. 3. Determination encapsulation efficiency of folic acid attached surface of liposomes. A) Standard curve of folic acid. B) Folic acid calibrating curve. C) Absorbance of free folic acid in the supernatant.

3.2. In vitro drug release study and loading capacity

Niacin and curcumin-loaded liposomal formulation exhibited continuous release during incubation at time intervals. The mechanism by which the drug can be released is mainly linked to the interaction of the material matrix and drugs, dissolution, drug diffusion, and physiological or chemical initiators [39].

In the current study, pure niacin and niacin-loaded liposomal formulation exhibited better release at pH 6.5 than at pH 7.4. This is due to the ability of niacin to be dissolved at lower pH. Niacin exhibited lower release in physiological pH 7.4 (Figs. 4 & 5).

The results indicated that the microenvironment of a tumor can stimulate niacin to be released out of a capsule. Because of its hydrophobic property, curcumin had a higher release at pH 6.5 than at pH 7.4. The accumulative drug release of encapsulated niacin and curcumin at pH 6.5 was about 60 % and 50 % after 72 h incubation respectively. Such liposomal interactions can be ionized at acidic pH, thereby releasing the drug effectively to target cancer cells.

Meanwhile, the accumulative release of niacin loaded liposomes alone achieved 90 % after 72 h incubation. This is due to the hydrophobic behavior of CUR that could minimize the release of niacin. In contrarily, the accumulative drug release of encapsulated niacin and curcumin at pH 7.2 was estimated at 15 % and 10 % after 72 h incubation.

In the current study, niacin and curcumin were released continuously throughout the time of incubation compared to free niacin and curcumin incubated separately. The results revealed the possible re-

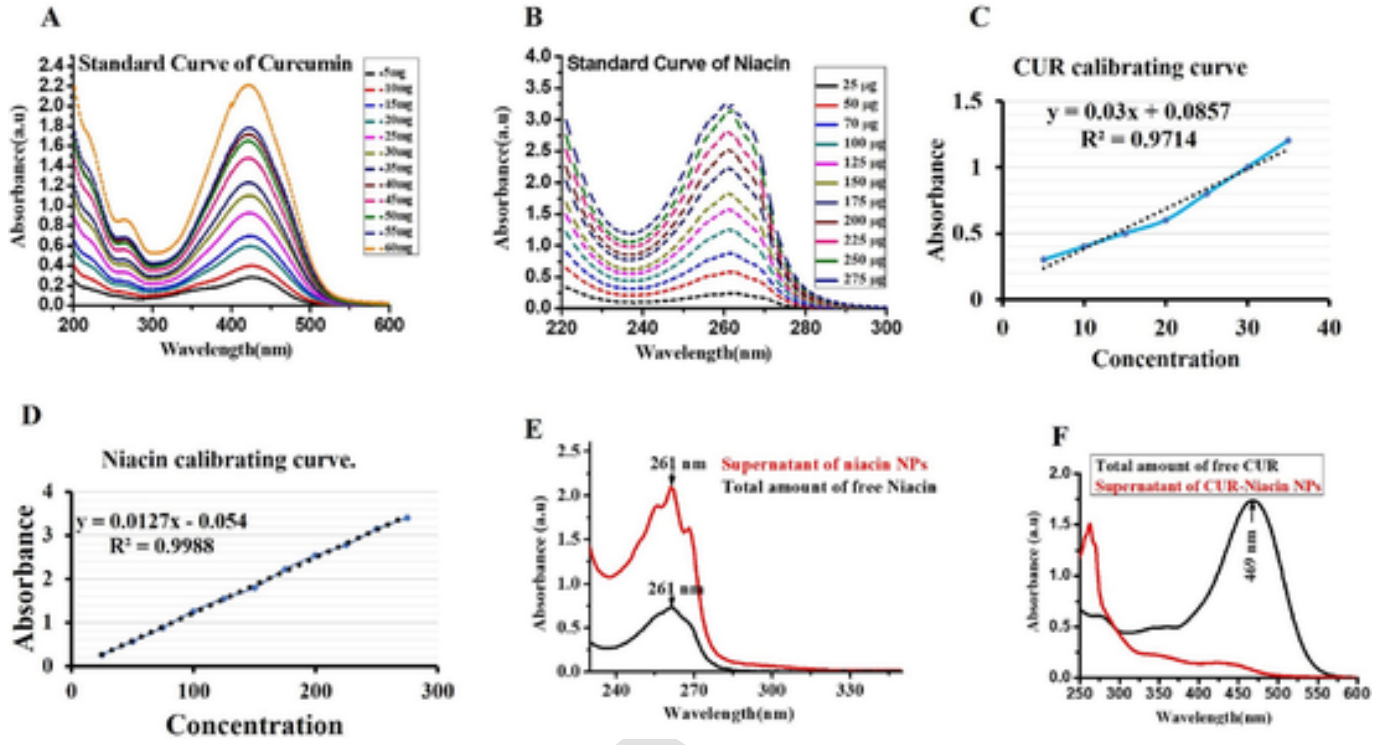

Fig. 4. A: Standard curve of curcumin. B: Standard curve of niacin. C: Graph of curcumin calibrating curve. D. Graph of niacin calibrating curve. E: UV visible spectrophotometer showed absorbance of niacin in supernatant compared to total free of niacin. F: UV visible spectrophotometer showed absorbance of CUR in supernatant compared to total free of CUR.

lease of niacin and curcumin-loaded liposomal formulation after their internalization (Fig. 6; A-B and Table 4).

The result is in agreement with Li et al. [15].who reported that pluronics modified liposomes could slow in vitro release of curcumin. While liposomes with no pluronics modification showed good release. Additionally, the strong interaction between curcumin and liposomal bilayers can minimize its release in physiological pH 7.4 compared to pH.6.5. the current result was not in the line of De Leo et al. who showed that curcumin-loaded liposome suspension (1 mL, pH 7.4) was released completely after 200 min incubation with oleic acid at 25 °C [17]. This is due to the absence of polymer modification in the liposomal formulation.

Niacin loaded liposomal NPs obtained higher encapsulation efficiency (EE%) reaching 96.2 ± 1.6 %. This is due to the interaction of the niacin carboxylic group with an amino group of chitosan during fabrication. Meanwhile, CUR-loaded niacin liposomal formulation showed encapsulation efficiency reached 29 ± 2.3 % (Table 3). The total encapsulation efficiency (%) of Niacin/CUR entrapped liposomes was calculated according to [40] and exhibited 89 %.

The polydispersity index (PDI) and nanosized values were used as indicators to measure the stability of NPs incubated in different media. Niacin NPs and CUR-Niacin NPs obtained narrow size distribution after their incubation for 1 day and 5 days (Table 4). While their distribution exhibits a high dispersity in size with very abroad distribution when they were incubated in saline and DMEM for 1 day and 5 days. In contrast, CUR-Niacin NPs showed good stability in saline and DMEM. This means that salts, minerals, glucose, protein, and the other content of DMEM and saline could affect chitosan stability leading to protonate/deprotonate of chitosan (amino groups) that causes aggregation. However, CUR inserted into the liposomal shell stabilizes NPs from any aggregation [41].

3.3. In vitro studies

3.3.1. Cytotoxicity

The MTT assay is a popular colorimetric assay used extensively to measure cell viability and cell proliferation. It depends on the metabolic activity of nicotinamide adenine dinucleotide (NADPH)-dependent cellular oxidoreductase enzymes. The tetrazolium dye of the MTT reagent is reduced by the activity of this enzyme to its insoluble form, formazan, which has a purple color. Formazan is dissolved in DMSO and then the color is measured at 570 nm [42].

In this study, the MTT assay was used to estimate the percentage growth rate after incubation of HePG2 cells with serial concentrations (0.1,1,10,100, and 1000 μg/mL) of each of pure niacin, pure curcumin, niacin NPs, and curcumin-niacin NPs. Based on cellular proliferation, the results revealed that there was a significant inhibition of growth rate after 48 h of incubation at a concentration of 100 μg/mL by 91 % ± 1 %, $P \leq 0.002$ (pure niacin), 55 % ± 3 %, $P \leq 0.001$ (pure curcumin), 83 % ± 1.5 %, $P \leq 0.001$ (niacin NPs), and 51 % ± 1.5 % $P \leq 0.0001$ (curcumin-niacin NPs) of relative to the control (Fig. 6;C). The result was constant with [25] who reported that curcumin loaded liposomes exhibited the highest percentage of cell growth inhibition, with 90 % of cells killed within 72 h.

To confirm the potential therapeutic effect of CUR-niacin NPs and to use them later on an animal cancer model, the half-maximal inhibitory concentration (IC50) values for both Niacin pure, Niacin NPs, Curcumin pure and CUR-Niacin NPs were detected by using serial concentrations (0.1, 1, 10, 100, 1000 μg/mL) (Fig. 7). The result showed that Niacin pure and Niacin NPs have a low cytotoxic effect compared to curcumin pure that was expressed its cytotoxicity at IC50:515 μg/mL. For instance, the cytotoxicity was increased in HePG2 cell lines after their incubation with CUR-Niacin NPs (IC50: 233 μg/mL). The result confirms that niacin could increase the cytotoxicity of curcumin.

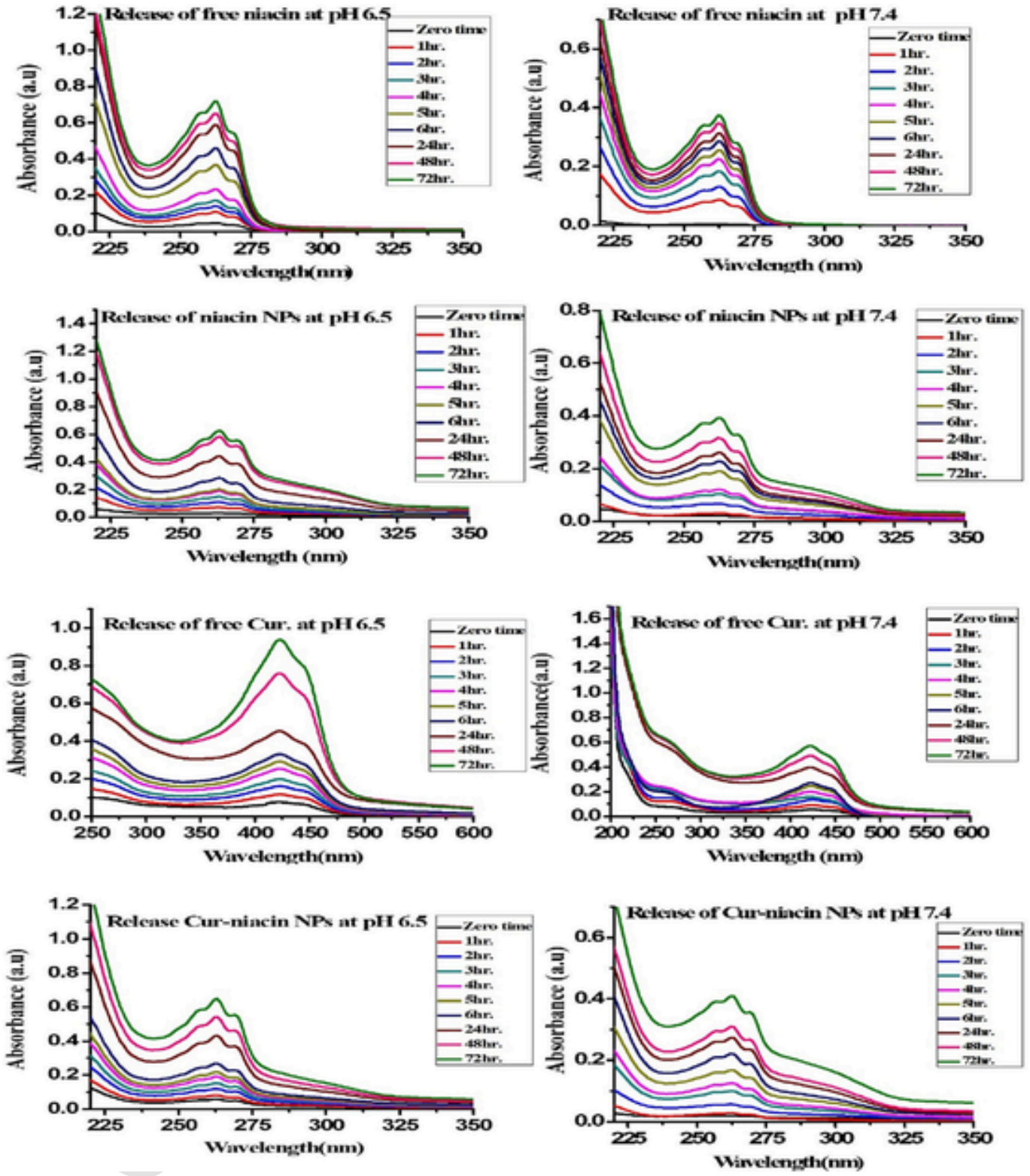

Fig. 5. Release of free niacin, niacin NPs, free curcumin, and curcumin-niacin NPs at pH 6.5 and pH 7.4.

3.3.2. Autophagy assay using flow cytometry

Flow cytometry is a sophisticated instrument measuring multiple physical characteristics of a single cell such as size and granularity simultaneously as the cell flows in suspension through a measuring device. Its working depends on the light scattering features of the cells under investigation, which may be derived from dyes or monoclonal antibodies targeting either extracellular molecules located on the surface or intracellular molecules inside the cell [43]. Forward versus side scatter (FSC vs. SSC) gating is commonly used to identify cells of interest based on size and granularity (complexity). It is often suggested that forward scatter indicates cell size whereas side scatter relates to the complexity or granularity of the cell [44].

In this study, the population of HePG2 cells was analyzed in two dimensions (forward scatter and side scatter) of flow cytometry after in-

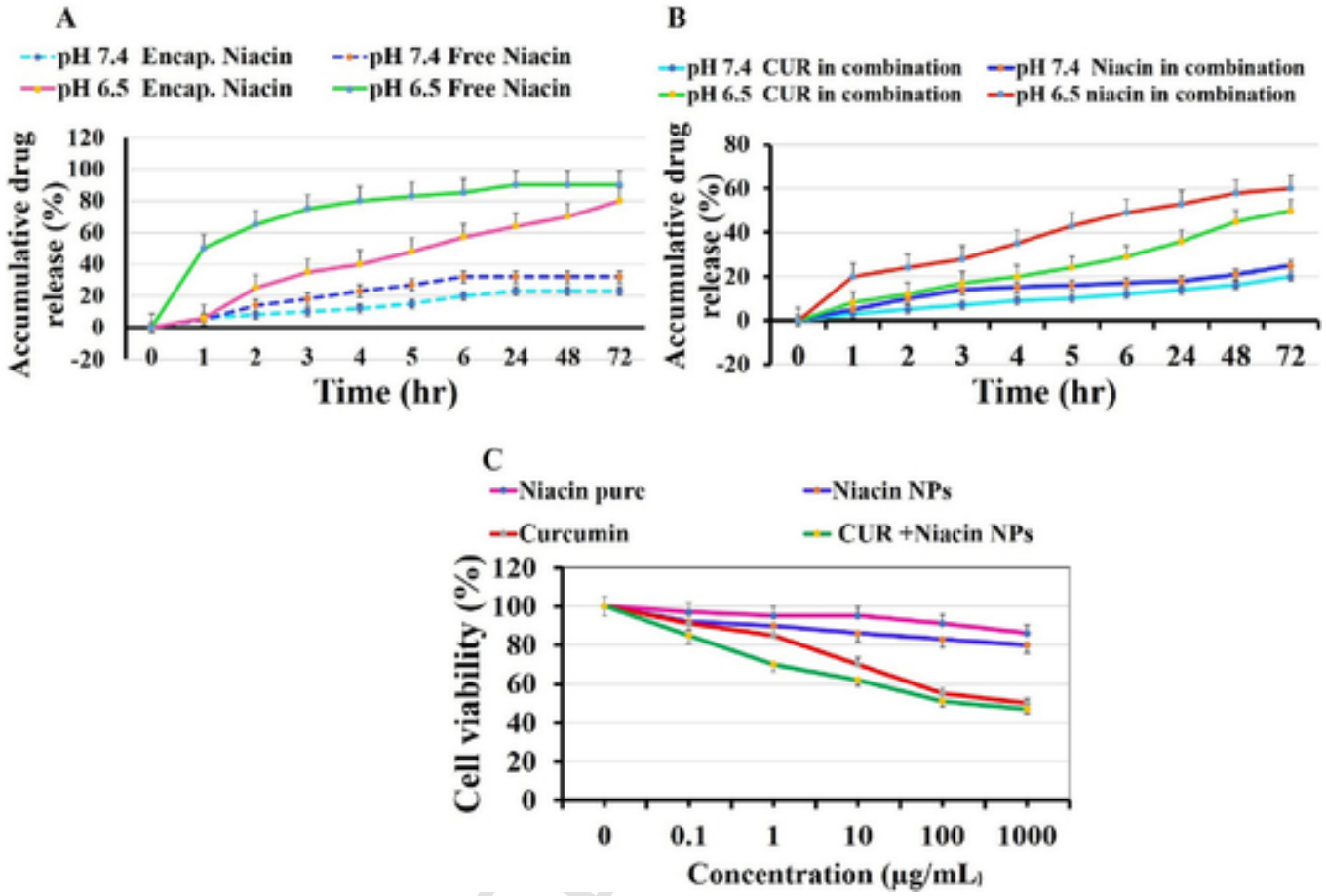

Fig. 6. A: Accumulative release of free niacin and Encap. Niacin at pH 6.5 and pH 7.4. B: Accumulative release of pure curcumin (CUR) and CUR-niacin NPs. C: Cell viability assay. The data are shown as the means ± SD ($n = 3$). * $p \leq 0.05$, and *** $p \leq 0.001$.

Table 3
Characterization of niacin NPs and CUR-niacin NPs.

Drug release	DLS (nm)	Zeta potential (mV)	PDI	Encapsulated Efficiency
Niacin from Niacin NPs	100 ± 9	−15 ± 0.3	0.359 ± 0.2	96.2 ± 1.6 %
CUR from CUR-Niacin NPs	240 ± 12	−42 ± 0.6	0.379 ± 0.25	29 ± 2.3 %

cubation for 48 h with pure niacin, pure curcumin, niacin NPs, and curcumin-niacin NPs. The results of flow cytometry showed that the forward scatter of AO-stained cells was shifted by 101 ± 1.2 μm and 96 ± 1.2 μm in pure niacin and niacin NPs, respectively relative to the control. There was not any change in side scatter [45]. Indeed, forward scatter is detected by a photodiode, which converts the light into an electrical signal. The intensity of the produced voltage is proportional to the diameter of the interrogated cell. For this reason, the shift of forward scatter can be detected by the diameter of the interrogated cell (μm).

In contrast, forward scatter was increased significantly by 181 ± 2.9 μm in HePG2 cells exposed to pure curcumin for 48 h. Additionally, the level of side scatter was increased relative to the control. The results revealed an increase in the number of granularity. Granularity indicates an increase in the number of autophagosomes [46]. Curcumin-loaded niacin NPs obtained significant shifting to forward scatter by 211 ± 1.2 μm and an increase in side scatter by 250 ± 1 relative to the control (Fig. 8) [47].

While the light reflection off of the granules increases the intensity of the SSC measurement and allows for discernment among many granulated cells. Thus discriminating of cells in side scatter can be proportional to their granules number.

Table 4
Stability of niacin NPs and CUR-niacin NPs in different media.

Nanoparticles	Distilled Water		Saline		DMEM	
	Hydrodynamic Size (nm)	PDI	Hydrodynamic Size (nm)	PDI	Hydrodynamic Size (nm)	PDI
After 1 day						
Niacin NPs	116 ± 4.3	0.352 ± 0.12	4154 ± 15	0.630 ± 0.3	1736 ± 22	0.415 ± 0.2
CUR-Niacin NPs	278 ± 5.8	0.336 ± 0.2	692 ± 13	0.360 ± 0.21	819.9 ± 19	0.417 ± 0.3
After 5 days						
Niacin NPs	134 ± 3.2	0.096 ± 0.01	16,330 ± 32	0.171 ± 0.05	1918 ± 33	0.526 ± 0.4
CUR-Niacin NPs	265 ± 4.6	0.321 ± 0.1	460 ± 17	0.087 ± 0.03	779 ± 21	0.509 ± 0.34

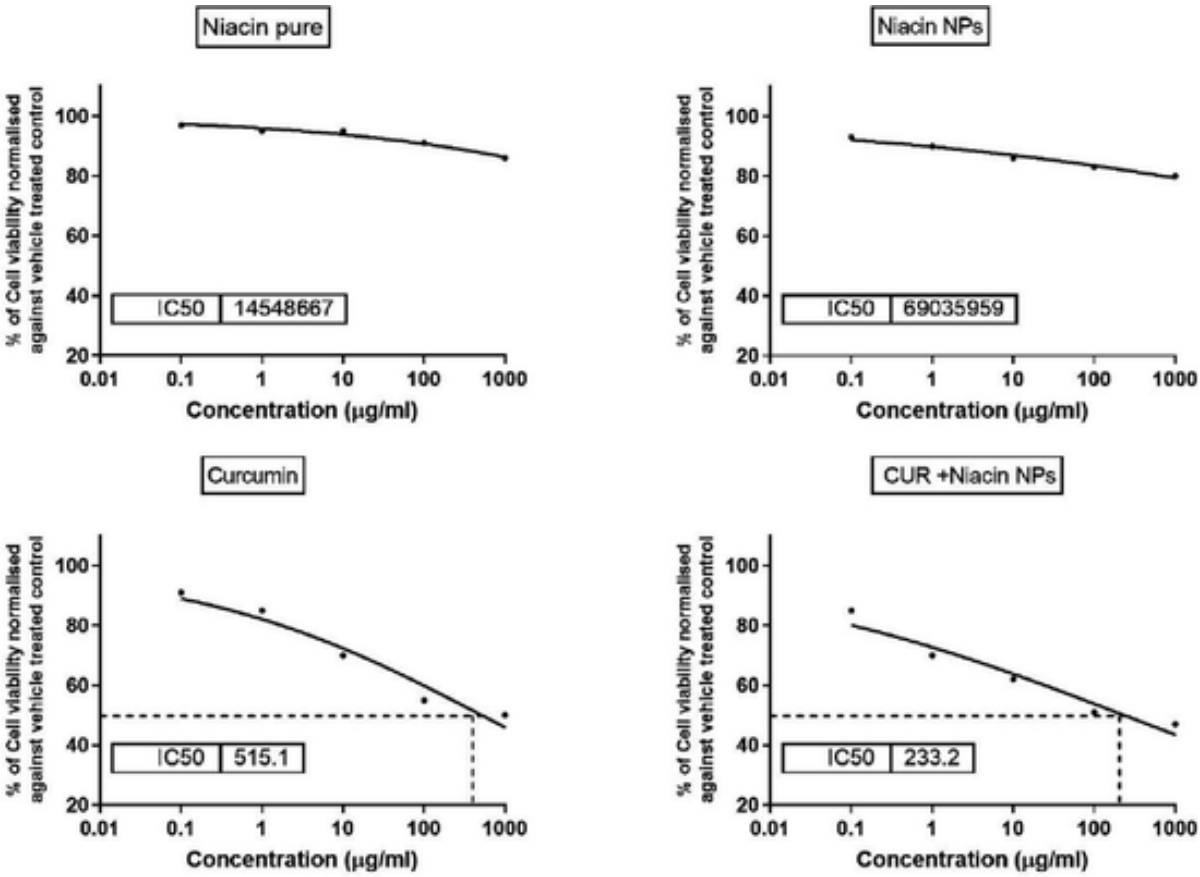

Fig. 7. IC50 of niacin pure, Niacin NPs, Curcumin pure and CUR-Niacin NPs on HePG2 cell lines.

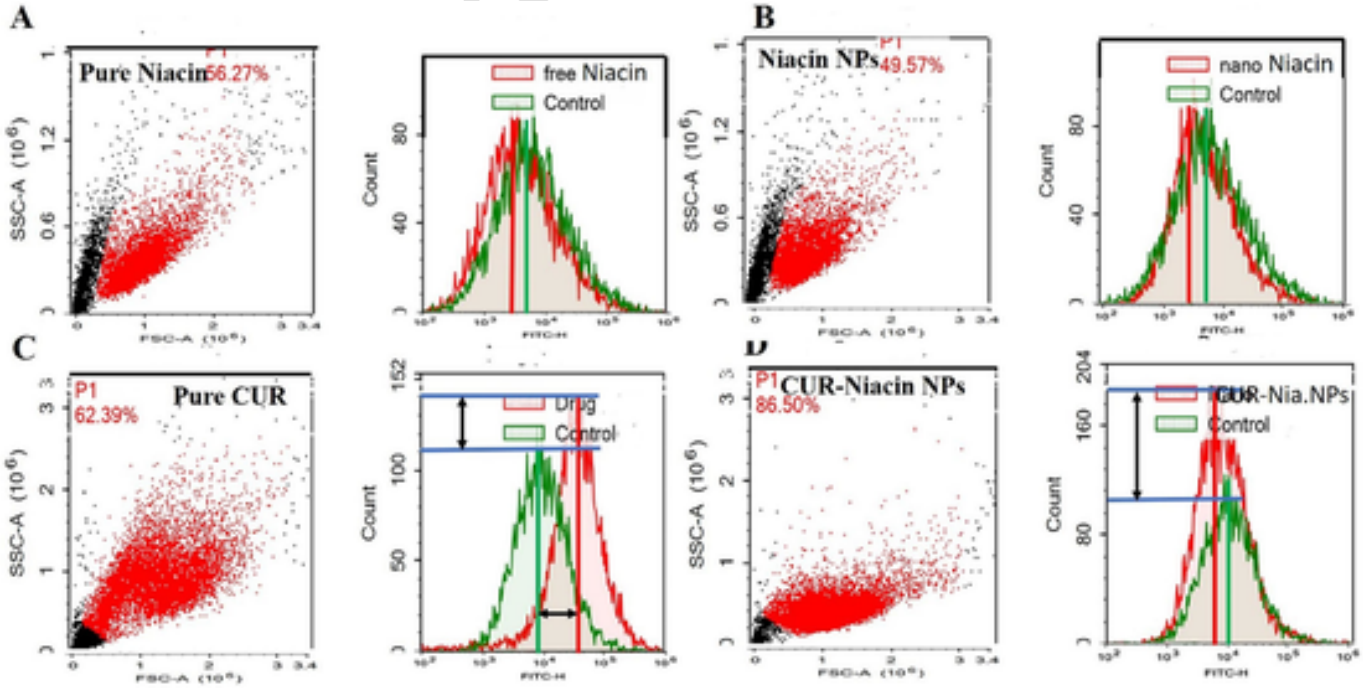

Fig. 8. Flow cytometric analysis of forward and side scatter of HePG2 cells exposed to pure niacin, niacin NPs, pure curcumin (CUR), and CUR-niacin NPs.

Based on cell size and complexity, the populations of HePG2 cells exposed to free niacin, free CUR, Niacin NPs, and CUR-Niacin NPs can be differentiated. The result showed that HePG2 displayed an increase in forward scatter and side scatter after their exposure to free CUR. It means that CUR leads to increase cells size and leads as well to increase number of granules inside the cytoplasm. While HePG2 cells exposed to free niacin or niacin NPs exhibited a shift in forward scatter with no change in side scatter. It means cell complexity and granularity disap-

peared after exposure HepG2 to niacin or niacin NPs. Nevertheless, niacin or niacin NPs caused a lower forward scatter. The result indicates that niacin had markedly lower cell volume but did not affect cell mass. The data is in agreement with the above results of cytotoxicity assay showing that the proliferation of HepG2 obtained 91 % ± 1 %, $P \leq 0.002$ (pure niacin) and 83 % ± 1.5 %, $P \leq 0.001$ (niacin NPs) compared to pure curcumin (55 % ± 3 %, $P \leq 0.001$) and curcumin-niacin NPs (51 % ± 1.5 % $P \leq 0.0001$).

3.3.3. Evaluation of gene expression using RT-PCR

3.3.3.1. ATG7 (autophagy related 7). ATG7 is an essential autophagy effector enzyme that, in concert with other ATG proteins, also regulates immunity, cell death and protein secretion, and independently regulates the cell cycle and apoptosis. The gene Atg7 is essential for ATG12 conjugation, LC3 modification systems, and autophagosome formation in mammals [48].

In this study, the relative expression level of ATg7 mRNA was significantly downregulated by 1.1 ± 0.1 $P \leq 0.0001$, 0.73 ± 0.06 $P \leq 0.0001$, 1.62 ± 0.07, $P \leq 0.01$ and 0.73 ± 0.07, $P \leq 0.0001$ folds after treatment of HepG2 cells with pure niacin, pure curcumin, niacin NPs, and curcumin -niacin NPs, respectively, relative to the control (1.9 ± 0.1) (Fig. 9; A). These results were in accordance with those published by [49] suggesting the activation of autophagy via the NRF-2 signaling pathway.

3.3.3.1.1. Beclin-1. Beclin-1 is the mammalian homolog of yeast Atg6 involved in autophagy and tumor suppression, often deleted in ovarian and breast cancer [50]. In this study, the treatment of HepG2 cells with pure niacin, pure CUR, Niacin NPs and CUR-niacin NPs re significant reduction in the expression of Beclin1 mRNA by (2 ± 0.1 $P \leq 0.001$, 1.7 ± 0.08 $P \leq 0.0001$, 2.1 ± 0.1 $P \leq 0.004$and 1.2 ± 0.07 $P \leq 0.00001$folds) relative to the control (2.6 ± 0.07) (Fig. 9; B).

3.3.3.2. mTOR. Autophagy is controlled by the mechanistic target of rapamycin (mTOR), a key player in nutrient sensing and signaling and a classic example of a pleiotropic gene. mTOR acts upstream of transcription factors such as FOXO, NRF, and TFEB, controlling protein synthesis, degradation, and cellular growth, thereby regulating fertility as well as aging [51].

The results showed that the regulation of mTOR was overexpressed in HepG2 cells. The expression of mRNA of mTOR was significantly increased by 0.72 ± 0.08 P ≤ 0.001, 1 ± 0.1, 0. P ≤ 0.001, 5 ± 0.07 $P \leq 0.01$, and 1.3 ± 0.02 P ≤ 0.001 folds) in pure niacin, pure curcumin, niacin NPs and curcumin -niacin NPs, respectively, relative to the control with an expression of 0.3 ± 0.08 (Fig. 9; C) and (Scheme 2) [52].

3.3.3.2.1. p62. The protein p62 is an autophagy substrate that is used as a reporter of autophagy activity. It also delivers ubiquitinated proteins, such as tau, to the proteasome for degradation. In addition, it can shuttle between the nucleus and cytoplasm to bind with ubiquitinated cargoes and facilitate nuclear and cytosolic protein quality control. Other functions of p62 are gradually being discovered, emphasizing its importance in the proteolytic system [53].

Here, the overexpression of p62 mRNA was clearly shown after exposure of HepG2 cells to pure niacin, pure curcumin, niacin NPs, and curcumin-niacin NPs. The expression of p62 mRNA was significantly increased by 0.92 ± 0.07 $P \leq 0.05$, 1.7 ± 0.07 $P \leq 0.0001$, 0.72 ± 0.08 $P \leq 0.5$, and 2.1 ± 0.1 P ≤ 0.0001 folds relative to that of the control with an expression of 0.72 ± 0.08 (Fig. 9; D) and (Scheme 2) [54,55].

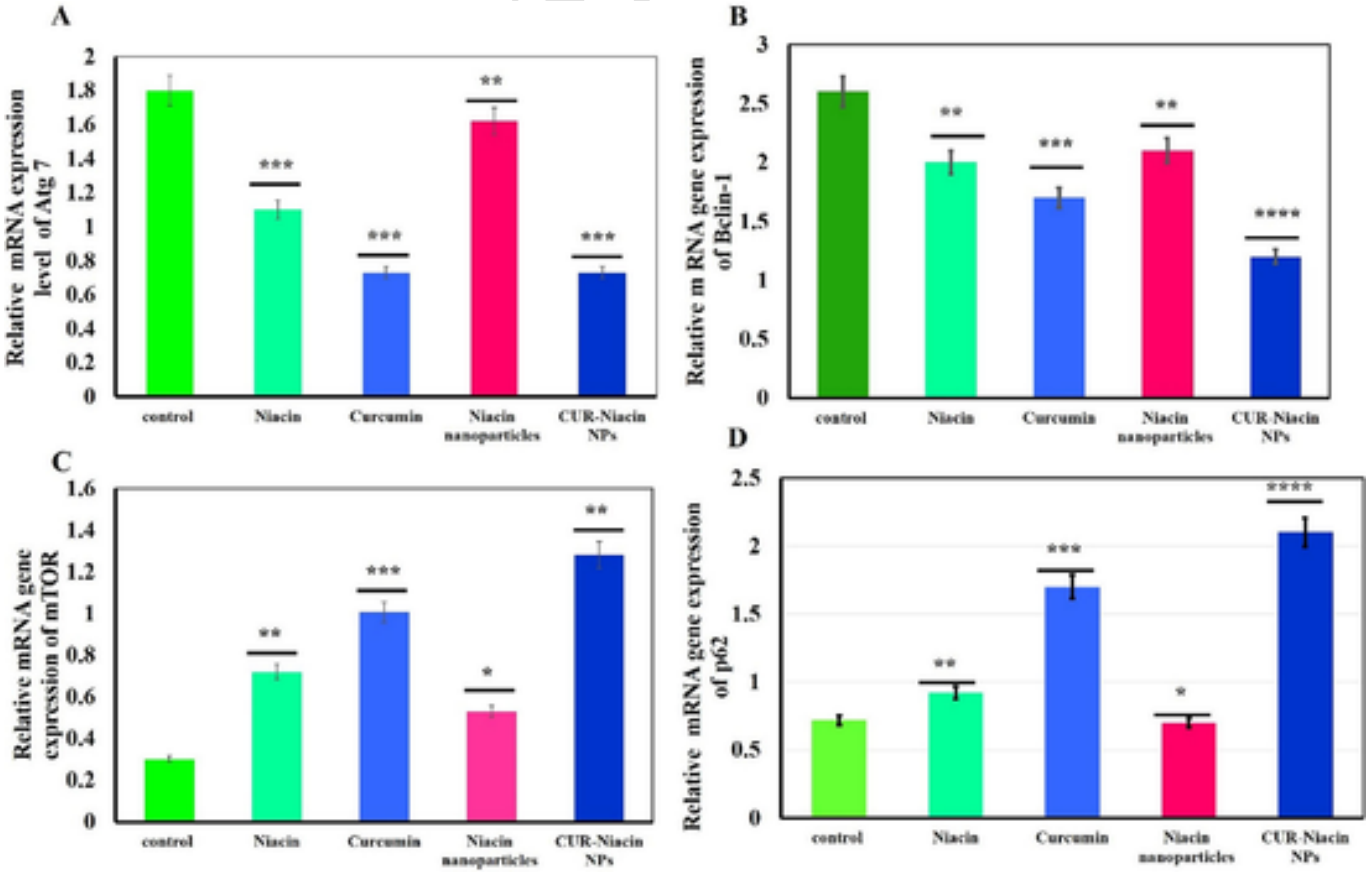

Fig. 9. Relative gene expression of ATG7 mRNA, Beclin-1, mTOR and p62 in HepG2 exposed to pure niacin, niacin NPs, curcumin (CUR), and CUR-niacin NP. The data are shown as the means ± SD ($n = 3$). * $p \leq 0.05$, ** $p \leq 0.01$, *** $p \leq 0.001$ and **** $p \leq 0.0001$.

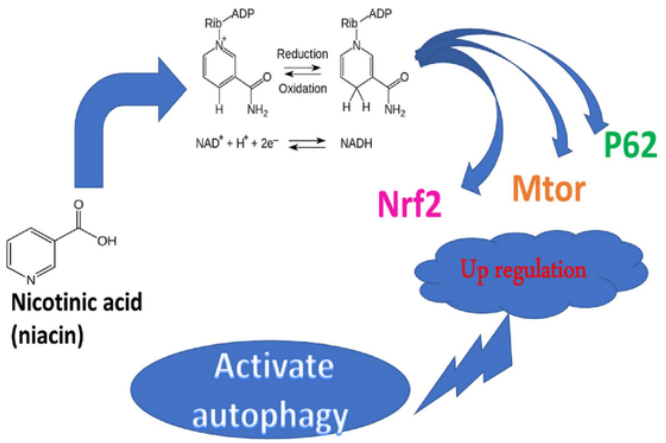

Scheme 2. Niacin can induce activation of mTOR, p62 and NRFs genes.

3.3.4. Cancer bio-image

3.3.4.1. AO/EB. The dual fluorescent stains (acridine orange/ethidium bromide (AO/EB)) can be used to identify cellular morphological changes associated with apoptotic and necrotic processes and autophagy [9]. Based on membrane integration, EB can penetrate into the cytoplasm and attach to DNA exposing nuclear alterations and chromatin condensation. In normal cells, the green color is imparted to DNA through AO intercalation in the presence of many acidic autophagosomes (red color). In the current study, the morphological alterations were visualized under fluorescence microscopy in pure niacin, pure curcumin, niacin NPs, and curcumin-niacin NPs. AO/EB showed a significant increase in cell size of HepG2 cells after their incubation with pure niacin 33.68 ± 5.7, $P \leq 0.007$), niacin NPs (43.27 ± 7.6, $P \leq 0.002$), pure curcumin (59.9 ± 10.8, $P \leq 0.001$), *and* curcumin - *niacin NPs* (*32.54* ± *3.06*, $P \leq 0.0005$) for 24 h relative to that of the control (22.74 ± 2.5). Before that, cells were observed with a rounded/ or semi-rounded shape emitting a slightly yellow color. In pure curcumin, nuclei of treated HepG2 cells were condensed and emitted a yellow-orange color. Curcumin-loaded niacin NPs exhibited nuclear degradation and many neutral autophagosomes were seen in the cytoplasm (Fig. 10) [56].

3.3.4.2. Cellular uptake and targeting capacity. The fluorescence microscopy images demonstrated that curcumin-loaded niacin NPs and niacin NPs accumulated in the cytoplasmic region of HepG2 cells. The overlapped channels of fluorescence microscopy revealed that characteristic yellow color resulting from the mixing of red (Rhodamine labeled capsules) and green (curcumin) accumulated in the cytoplasmic region (Fig. 11) [57]. The targeting capacity was measured by the intensity of accumulated NPs labeled by rhodamine. The corrected total cell fluorescence intensity after exposure of HePG2 cells to niacin NPs and curcumin -niacin NPs (with FA and without FA) was demonstrated and analyzed by the Image J program. The mean integration density was normalized to blank in the area of measurement. The results confirmed the accumulation of folic acid-conjugated NPs but not the non-conjugated ones.

4. Discussion

The activation of autophagy in cancer cells might open new insights into discovering and developing new strategies for cancer treatment be-

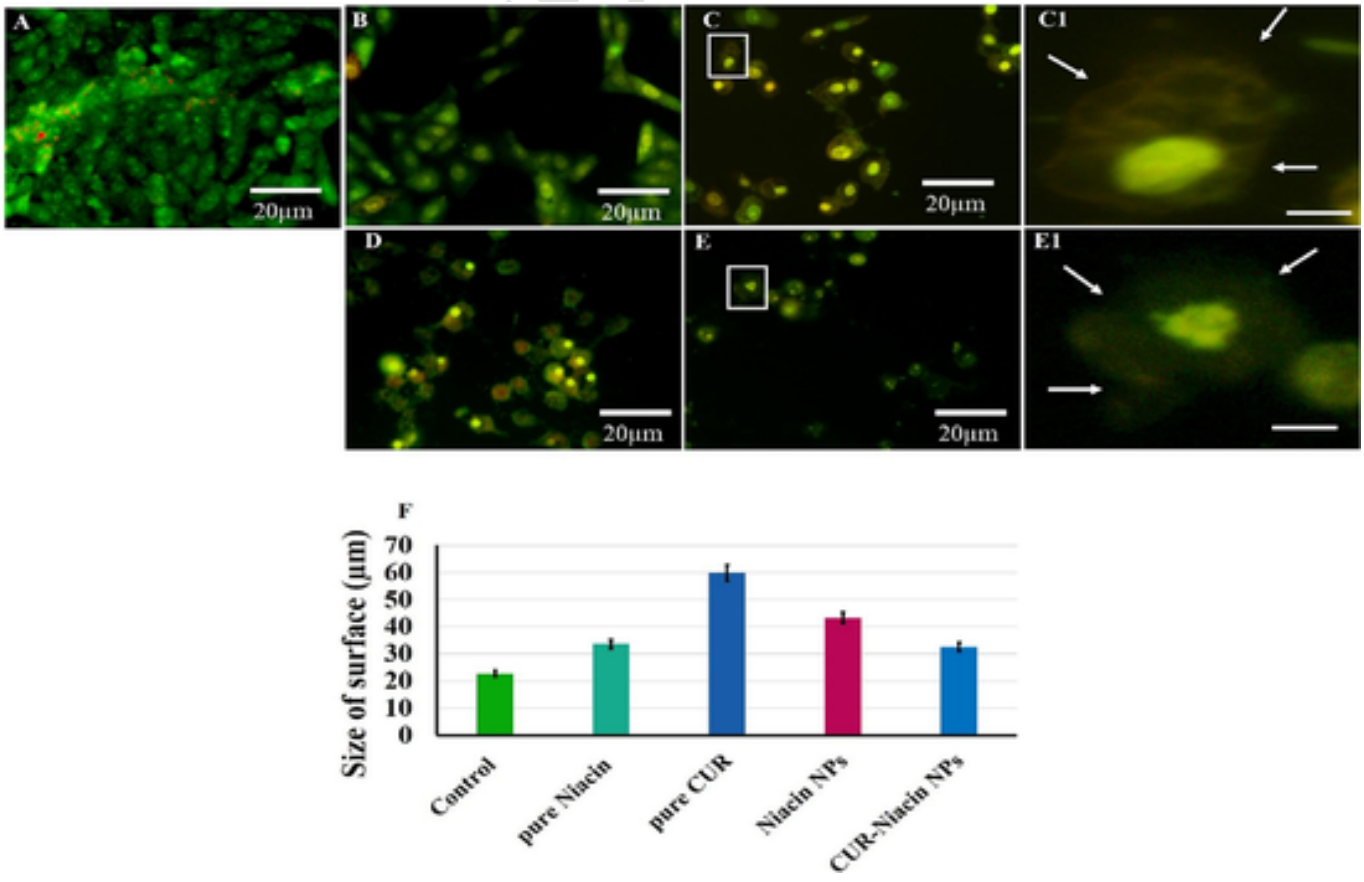

Fig. 10. Fluorescence microscopy showing morphology of HePG2 cells stained with AO/EB after their exposure to B: pure niacin, C: niacin NPs, D: curcumin(CUR), and E: CUR-niacin NPs relative to A: control. F: Quantification of size surface area by using image J program.

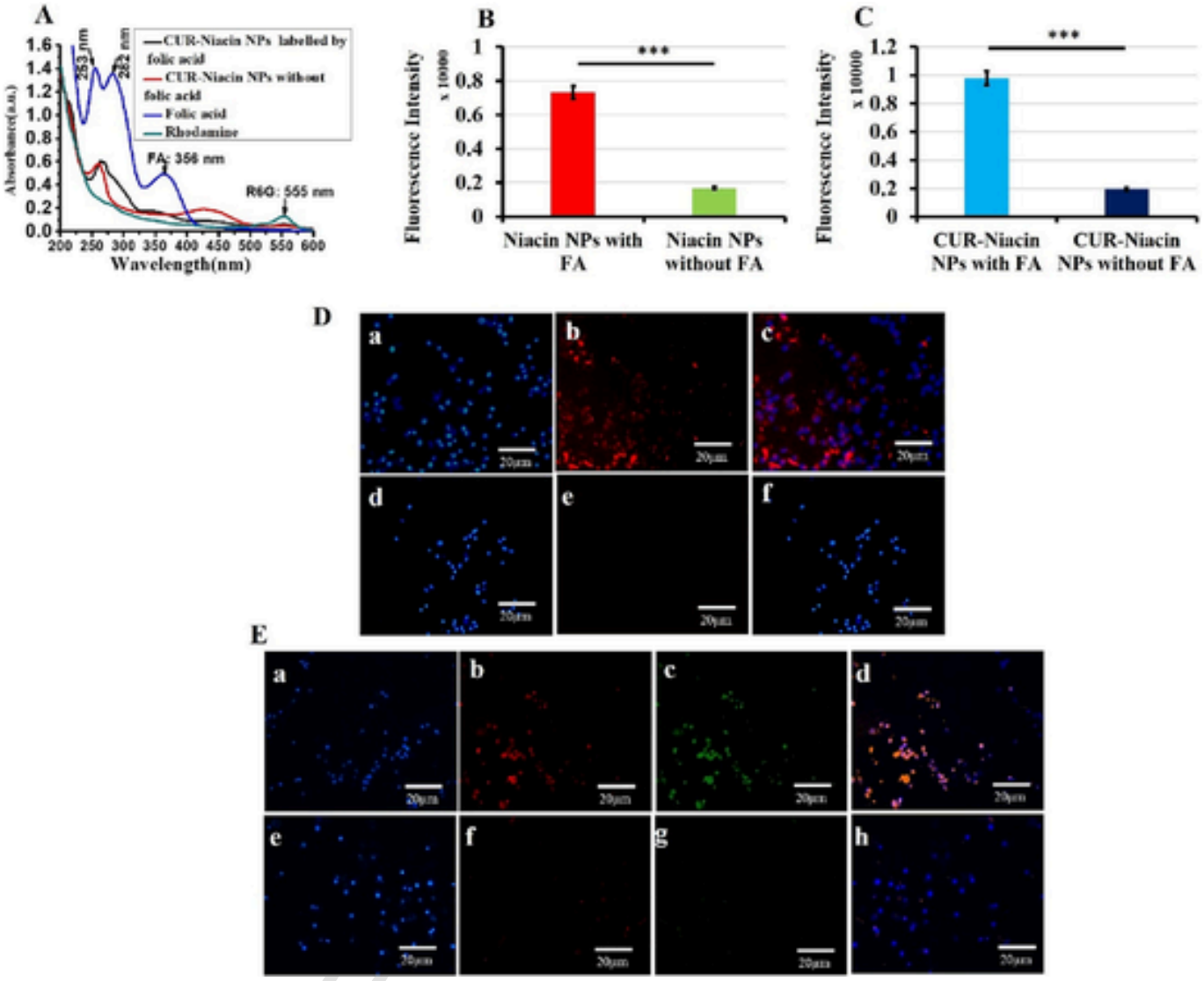

Fig. 11. Niacin NPs and curcumin (CUR)-niacin NPs were labeled with rhodamine. A: UV visible spectrophotometer showed conjugation of rhodamine with NPs. B: Quantification of the corrected total cell fluorescence intensity after exposure of HePG2 cells to niacin NPs and CUR-niacin NPs (with folic acid and without folic acid). D: Fluorescence microscopy images of HePG2 cells exposed to niacin NPs with folic acid (a-c) and niacin NPs without folic acid (d-f). E: Fluorescence microscopy images of HePG2 cells exposed to CUR-niacin NPs with folic acid (a-d), without folic acid (e-h). The data are shown as the means ± SD (n = 3)., *** $p \leq 0.001$.

cause of its ability to degrade intracellular cytoplasmic components by using lysosomal enzymatic degradation of the same cell [58]. Niacin can affect the mitochondrial complex 1 and enhance the NAD + /NADH ratio as reported by [59] in human breast adenocarcinoma cells. Additionally, it activates the PI3K/Akt cascade in the A431 human epithelial carcinoma cell line [60]. Vitamin B3 is an NAD + precursor that can increase intracellular NAD + concentrations. It mainly exists in the form of nicotinic acid (niacin), nicotinamide riboside, and nicotinamide [61]. There is a correlation between the ratio of [NAD +]/[NADH] with an increase in autophagy level [62].

In this study, our aim was to activate autophagy by using niacin and to increase the number of autophagosome using curcumin. To achieve this, curcumin and niacin-loaded targeted liposomes were characterized by TEM, FTIR, UV visible spectrophotometer, zeta potential, and dynamic light scattering [63]. The results showed well formulation of niacin-loaded targeted liposomes and curcumin-loaded niacin-targeted liposomes observing a spherical shape with nanosized diameter under TEM. The characteristic peaks of niacin adsorption were detected at 210 nm and 260 nm. These peaks were mainly shifted to 220 nm and 280 nm, respectively, after encapsulation (niacin NPs). Broad peaks were shown at 326 nm and 389 nm for CUR curcumin–niacin NPs spectrum after addition of curcumin. These peaks were attributed to both FA and curcumin adsorption. The functional chemical groups of curcumin were distributed upon the spectrum of curcumin-niacin NPs. A band at 3405 cm − 1 was a sign of stretching vibration of phenolic OH. A band at 1623 cm − 1 was shifted to 1648 cm-1 and a band at 1541 cm − 1 was shifted to 1557 cm − 1 after interaction with curcumin. Here, the MTT assay was used to explore the cytotoxicity of pure niacin, pure CUR, niacin NPs, and CUR-niacin NPs. The results showed a significant reduction in the growth of HePG2 cells by 91 % ± 1 %, $P \leq 0.002$; 55 % ± 3 %, $P \leq 0.001$; 83 % ± 1.5 %, P ≤ 0.001; and 51 % ± 1.5 % $P \leq 0.0001$, respectively, relative to that of the control.

Meanwhile, niacin NPs and CUR-niacin NPs exhibited good drug release as shown in (Table 5).

In order to understand the mechanism by which pure niacin, pure curcumin, niacin NPs, and curcumin-niacin NPs can modulate cellular pathway compared to untreated HePG2 cells, we used flow cytometry, RT-PCR for gene expression, and dual fluorescent microscopy stains

Table 5
The % of accumulative drug release after incubation for 72 h in physiological pH 7.2 and microenvironment pH 6.5.

Niacin/CUR	pH 6.5	pH 7.2
Niacin in combination	60 ± 2.3 %	15 ± 1.6 %
CUR in combination	50 ± 1.5 %	10 ± 1.4 %
Niacin encapsulated separately	80 ± 3.2 %	10 ± 0.9 %
Free Niacin	90 ± 3.4 %	10 ± 1.2 %

(AO/EB). Flow cytometric analyses of HePG2 cells showed a reduction in forward scattering (an indication of cell size [64]) without any change in side scatter. Curcumin-Niacin NPs significantly increased side scatter (an indication of granularity [65,66]).

To explore the expression of gene mediated autophagy, regulation of ATG7, Beclin 1, mTOR, and p62 were evaluated in HePG2 cells exposed to pure niacin, pure curcumin, Niacin NPs, and curcumin-niacin NPs relative to that of the control. The results showed significant reduction in the relative expression levels of ATG7 mRNA and Beclin-1. The current results are in full agreement with those of [46] who reported that nician can induce a reduction of gene expression of ATG5, ULK1, ATG4B, Beclin, LC3B, and ATG7. Niacin can regulate NRF-2/HO-1 signaling via activation of the GPR109A receptor. The activation of GPR109A might promote autophagy via the NRF-2 signaling pathway [46]. In contrast, the results showed a significant increase in the mTOR in response to pure niacin, pure curcumin, Niacin NPs, and curcumin-niacin NPs. This is mainly in agreement to the findings of [67] who reported that autophagic recycling of cellular components results in the reactivation of mTORC1.

Likewise, the expression of the mRNA p62 level, a protein encoded by the sequestosome 1 gene (SQSTM1), was upregulated in HePG2 cells exposed to pure niacin, pure curcumin, niacin NPs, and curcumin-niacin NPs relative to that of the control. Similarly, HePG2 cells treated with sorafenib showed a significant increase in p62 gene expression [68,69]. In previous studies, expression of p62 was significantly upregulated in prostate cancer, gastric cancer, lung cancer, colorectal cancer, pancreatic cancer, skin melanoma, and diffuse large b-cell lymphoma, relative to that of normal tissues. Therefore, p62 can contribute to drug resistance because of its ability to decrease the activation of autophagy, thereby promoting the survival of HCC cells in sorafenib treated HePG2 cells [70]. In spite of its role in impairing autophagy, p62 activates Nrf2 and mTOR pathways that play a role in the direct activation of autophagy via phosphorylation of the GPR109A receptor. The protein p62 is assembled on selective autophagic cargoes such as ubiquitinated organelles and subsequently phosphorylated in a mTORC1-dependent manner, implying coupling of the Keap1-Nrf2 system to autophagy [71].

The limitation of the CUR-Niacin NPs method was shown in the fabrication process. Since curcumin can induce aggregation in the liposomal formulation at the time of the process. For this reason, the mixture should be sonicated for 3 min. and curcumin should be added slowly. The other limitation that could be highlighted here is related to the concentration of curcumin inside moieties of the liposomal formulation. The loading capacity of curcumin was calculated as 29 %. Nevertheless, this concentration is more logical mean because curcumin was encapsulated in layers of liposome.

It can be summarized that the toxicity of chemotherapies was studied extensively for carboplatin, doxorubicin, irinotecan, carboplatin, vinorelbine, and topotecan which is due to their poor cellular adsorption and low selectivity. For this reason, the application of drug delivery systems loaded with natural products in cancer treatment is highlighted because of their simple and ease of fabrication. In this case, this strategy can be used to overcome the limitations of curcumin in cancer therapy because of its extremely low solubility in aqueous buffer, instability in body fluids, and rapid metabolism.

5. Conclusion

Evidence suggesting a role of autophagy in drug resistance and promoting survival of cancer cells is accumulating. Previous studies have confirmed that niacin can increase intracellular NAD+ concentrations, and activate NRF-2 and mTOR signaling pathways. These findings suggest that niacin can induce autophagy by activating the GPR109A/AMPK/NRF-2 signaling pathway. In this study, pure niacin, pure curcumin, Niacin NPs, and curcumin-niacin NPs were used to treat HePG2 cells. The results confirmed the upregulation of mTOR and p62 expressions and the downregulation of ATG7 and Beclin-1 expressions. Additionally, flow cytometric analysis and AO/EB microscopic image confirmed activation of autophagy [72–74].

Ethics approval and consent to participate

All experiments were conducted in accordance with US National Institutes of Health Guidelines for the Care and Use of Laboratory Animals and cell line experiments Guide for the Care and Use of Laboratory Animals after being approved by the relevant Ethical Committee and authorized by the Italian and German Ministry of Health. This study was also approved by the Research Ethics Committee of Kafrelsheikh University.

Consent for publication

All authors have provided their agreement to publish the submitted manuscript.

Funding

This research received no any funds.

CRediT authorship contribution statement

NANH: Methodology, data curation, investigation, writing original draft, preparation, design the manuscript, format analysis and supervision. RFS: Methodology, data curation, investigation, format analysis, write original draft. EAM: Investigation, design the manuscript, reviewing and editing original draft, supervision, MEM: Supervision, review and editing, investigation, design the manuscript. All authors have read and agreed to the published version of the manuscript.

Authors' information

Data of authors will be available in proof reading manuscript after being accepted.

Declaration of competing interest

The authors declare no conflict of interest.

Data availability

Data available in a publicly accessible repository.

Acknowledgements

Reha Fouad Sheashaa would like to thank professor Dr. Magdy E. Mahfouz and Eman A. Moussa for their kind supervision, support, and their encouragement, and Nemany A.N. Hanafy for his great supervision and his ability to facilitate all my practical work and did not save any effort or time to support me in accomplishing this work.

Appendix A. Supplementary data

Supplementary data to this article can be found online at https://doi.org/10.1016/j.ijbiomac.2023.125572.

References

[1] M. Renzulli, A. Pecorelli, N. Brandi, G. Marasco, F. Adduci, F. Tovoli, B. Stefanini, A. Granito, R. Golfieri, Radiological features of microvascular invasion of hepatocellular carcinoma in patients with non-alcoholic fatty liver disease, Gastroenterol. Insights 13 (2022) 275–285, https://doi.org/10.3390/gastroent13030028.

[2] A.H. Ibrahim, E. Shash, General oncology Care in Egypt, in: H.O. Al-Shamsi, I.H. Abu-Gheida, F. Iqbal, A. Al-Awadhi (Eds.), Cancer in the Arab world, Springer, Singapore, 2022, https://doi.org/10.1007/978-981-16-7945-2_4.

[3] D.W. Kim, C. Talati, R. Kim, Hepatocellular carcinoma (HCC): beyond sorafenib-chemotherapy, J. Gastrointest. Oncol. 8 (2) (2017 Apr) 256–265 https://doi.org/10.21037/jgo.2016.09.07 (PMID: 28480065).

[4] S.W. Kim, J.H. Lee, J.H. Moon, U.M. Nazim, Y.J. Lee, J.W. Seol, J. Hur, S.K. Eo, J.H. Lee, S.Y. Park, Niacin alleviates TRAIL-mediated colon cancer cell death via autophagy flux activation, Oncotarget. 7 (4) (2016 Jan 26) 4356–4368, https://doi.org/10.18632/oncotarget.5374. PMID: 26517672.

[5] T. Su, X. Li, M. Yang, Q. Shao, Y. Zhao, C. Ma, P. Wang, Autophagy: an intracellular degradation pathway regulating plant survival and stress response, Front. Plant Sci. 11 (2020 Feb 28) 164, https://doi.org/10.3389/fpls.2020.00164.

[6] D. Kong, Z. Zhang, L. Chen, W. Huang, F. Zhang, L. Wang, Y. Wang, P. Cao, S. Zheng, Curcumin blunts epithelial-mesenchymal transition of hepatocytes to alleviate hepatic fibrosis through regulating oxidative stress and autophagy, Redox Biol. 36 (2020 Sep) 101600, https://doi.org/10.1016/j.redox.2020.

[7] H. Song, C. Su, W. Cui, B. Zhu, L. Liu, Z. Chen, L. Zhao, Folic acid-chitosan conjugated nanoparticles for improving tumor-targeted drug delivery, Biomed. Res. Int. 2013 (2013) 723158, https://doi.org/10.1155/2013/723158.

[8] N.A.N. Hanafy, M.A. El-Kemary, Silymarin/curcumin loaded albumin nanoparticles coated by chitosan as muco-inhalable delivery system observing anti-inflammatory and anti COVID-19 characterizations in oleic acid triggered lung injury and in vitro COVID-19 experiment, Int. J. Biol. Macromol. 198 (2022 Feb 15) 101–110, https://doi.org/10.1016/j.ijbiomac.2021.

[9] N.A.N. Hanafy, S. Leporatti, M.A. El-Kemary, Extraction of chlorophyll and carotenoids loaded into chitosan as potential targeted therapy and bio imaging agents for breast carcinoma, Int. J. Biol. Macromol. 182 (2021 Jul 1) 1150–1160, https://doi.org/10.1016/j.ijbiomac.2021.03.189.

[10] N.A.N. Hanafy, Optimally designed theranostic system based folic acids and chitosan as a promising mucoadhesive delivery system for encapsulating curcumin LbL nano-template against invasiveness of breast cancer, Int. J. Biol. Macromol. 182 (2021) 1981–1993.

[11] N.A.N. Hanafy, M. El-Kemary, S. Leporatti, Mucoadhesive curcumin crosslinked carboxy methyl cellulose might increase inhibitory efficiency for liver cancer treatment, Mater. Sci. Eng. C. 116 (2020) 111119.

[12] N.A.N. Hanafy, I. Fabregat, S. Leporatti, M.E. Kemary, Encapsulating TGF-β1 inhibitory peptides P17 and P144 as a promising strategy to facilitate their dissolution and to improve their functionalization, Pharmaceutics 12 (2020) 421.

[13] S. Naeem, L.V. Kiew, L.Y. Chung, et al., A comparative approach for the preparation and physicochemical characterization of lecithin liposomes using chloroform and non-halogenated solvents, J. Surfact. Deterg. 18 (2015) 579–587, https://doi.org/10.1007/s11743-015-1689-3.

[14] C. Cheng, S. Peng, Z. Li, W. Liu, C. Liu, Improved bioavailability of curcumin in liposomes prepared using a pH-driven, organic solvent-free, easily scalable process, RSC Adv. 7 (2017) (25978–2598).

[15] Z.L. Li, S.F. Peng, X. Chen, Y.Q. Zhu, L.Q. Zou, W. Liu, C.M. Liu, Pluronics modified liposomes for curcumin encapsulation: sustained release, stability and bioaccessibility, Food Res. Int. 108 (2018 Jun) 246–253, https://doi.org/10.1016/j.foodres.2018.03.048.

[16] H. He, Y. Lu, J. Qi, W. Zhao, X. Dong, W. Wu, Biomimetic thiamine- and niacin-decorated liposomes for enhanced oral delivery of insulin, Acta Pharm. Sin. B 8 (1) (2018 Jan) 97–105, https://doi.org/10.1016/j.apsb.2017.11.007.

[17] V. De Leo, F. Milano, E. Mancini, R. Comparelli, L. Giotta, A. Nacci, F. Longobardi, A. Garbetta, A. Agostiano, L. Catucci, Encapsulation of curcumin-loaded liposomes for colonic drug delivery in a pH-responsive polymer cluster using a pH-driven and organic solvent-free process, Molecules 23 (4) (2018 Mar 23) 739, https://doi.org/10.3390/molecules23040739.

[18] M. Huang, C. Liang, C. Tan, S. Huang, R. Ying, Y. Wang, Z. Wang, Y. Zhang, Liposome co-encapsulation as a strategy for the delivery of curcumin and resveratrol, Food Funct. 10 (10) (2019 Oct 16) 6447–6458, https://doi.org/10.1039/c9fo01338e.

[19] C. Schmitt, A. Lechanteur, F. Cossais, C. Bellefroid, P. Arnold, R. Lucius, J. Held-Feindt, G. Piel, K. Hattermann, Liposomal encapsulated curcumin effectively attenuates neuroinflammatory and reactive astrogliosis reactions in glia cells and organotypic brain slices, Int. J. Nanomedicine 15 (2020 May 25) 3649–3667, https://doi.org/10.2147/IJN.S245300.

[20] X.Q. Wei, J.F. Zhu, X.B. Wang, K. Ba, Improving the stability of liposomal curcumin by adjusting the inner aqueous chamber pH of liposomes, ACS Omega 5 (2) (2020 Jan 7) 1120–1126, https://doi.org/10.1021/acsomega.9b03293.

[21] A. López-Machado, N. Díaz-Garrido, A. Cano, M. Espina, J. Badia, L. Baldomà, A.C. Calpena, E.B. Souto, M.L. García, E. Sánchez-López, Development of lactoferrin-loaded liposomes for the management of dry eye disease and ocular inflammation, Pharmaceutics. 13 (10) (2021 Oct 15) 1698, https://doi.org/10.3390/pharmaceutics13101698.

[22] M. Estephan, R. El Kurdi, D. Patra, Interaction of curcumin with diarachidonyl phosphatidyl choline (DAPC) liposomes: chitosan protects DAPC liposomes without changing phase transition temperature but impacting membrane permeability, Colloids Surf. B Biointerf. 199 (2021 Mar) 111546, https://doi.org/10.1016/j.colsurfb.2020.111546.

[23] J.W. Song, Y.S. Liu, Y.R. Guo, W.X. Zhong, Y.P. Guo, L. Guo, Nano-liposomes double loaded with curcumin and tetrandrine: preparation, characterization, hepatotoxicity and anti-tumor effects, Int. J. Mol. Sci. 23 (12) (2022 Jun 20) 6858, https://doi.org/10.3390/ijms23126858.

[24] H. Quach, T.V. Le, T.T. Nguyen, P. Nguyen, C.K. Nguyen, L.H. Dang, Nano-lipids based on ginger oil and lecithin as a potential drug delivery system, Pharmaceutics 14 (8) (2022 Aug 9) 1654, https://doi.org/10.3390/pharmaceutics14081654.

[25] A.K. Othman, R. El Kurdi, A. Badran, J. Mesmar, E. Baydoun, D. Patra, Liposome-based nanocapsules for the controlled release of dietary curcumin: PDDA and silica nanoparticle-coated DMPC liposomes enhance the fluorescence efficiency and anticancer activity of curcumin, RSC Adv. 12 (18) (2022 Apr 11) 11282–11292, https://doi.org/10.1039/d2ra00071g.

[26] V. De Leo, A.M. Maurelli, L. Giotta, V. Daniello, S. Di Gioia, M. Conese, C. Ingrosso, F. Ciriaco, L. Catucci, Polymer encapsulated liposomes for oral co-delivery of curcumin and hydroxytyrosol, Int. J. Mol. Sci. 24 (1) (2023 Jan 2) 790, https://doi.org/10.3390/ijms24010790.

[27] H. Quach, T.V. Le, T.T. Nguyen, P. Nguyen, C.K. Nguyen, L.H. Dang, Nano-lipids based on ginger oil and lecithin as a potential drug delivery system, Pharmaceutics 14 (8) (2022 Aug 9) 1654, https://doi.org/10.3390/pharmaceutics14081654.

[28] Mabrouk Zayed, Mayada Mohamed, Heba A. Sahyon, Nemany A.N. Hanafy, Maged A. El-Kemary, The effect of encapsulated Apigenin nanoparticles on HePG-2 cells through regulation of P53, Pharmaceutics 14 (6) (2022) 1160, https://doi.org/10.3390/pharmaceutics14061160.

[29] J.M. Kim, I.H. Hwang, I.S. Jang, M. Kim, I.S. Bang, S.J. Park, Y.J. Chung, J.C. Joo, M.G. Lee, Houttuynia cordata thunb promotes activation of HIF-1A-FOXO3 and MEF2A pathways to induce apoptosis in human HepG2 hepatocellular carcinoma cells, Integr. Cancer Ther. 16 (3) (2017 Sep) 360–372, https://doi.org/10.1177/1534735416670987.

[30] F.C.P. Freitas, T.S. Depintor, L.T. Agostini, et al., Evaluation of reference genes for gene expression analysis by real-time quantitative PCR (qPCR) in three stingless bee species (Hymenoptera: Apidae: Meliponini), Sci. Rep. 9 (2019) 17692, https://doi.org/10.1038/s41598-019-53544-0.

[31] A.F. Aisha, A.M. Majid, Z. Ismail, Preparation and characterization of nano liposomes of Orthosiphon stamineus ethanolic extract in soybean phospholipids, BMC Biotechnol. 14 (2014) 23, https://doi.org/10.1186/1472-6750-14-23.

[32] N. Aibani, R. Rai, P. Patel, G. Cuddihy, E.K. Wasan, Chitosan nanoparticles at the biological interface: implications for drug delivery, Pharmaceutics 13 (10) (2021 Oct 14) 1686, https://doi.org/10.3390/pharmaceutics13101686.

[33] A.F. Aisha, A.M. Majid, Z. Ismail, Preparation and characterization of nano liposomes of orthosiphon stamineus ethanolic extract in soybean phospholipids, BMC Biotechnol. 14 (2014) 23, https://doi.org/10.1186/1472-6750-14-23.

[34] M. Hasanin, A.M., Labeeb dielectric properties of nicotinic acid/methyl cellulose composite via "green" method for anti-static charge applications, Mater. Sci. Eng. B 263 (2021), https://doi.org/10.1016/j.mseb.2020.114797.

[35] S. Mourdikoudis, R.M. Pallares, N.T.K. Thanh, Characterization techniques for nanoparticles: comparison and complementarity upon studying nanoparticle properties, Nanoscale 10 (27) (2018 Jul 13) 12871–12934, https://doi.org/10.1039/c8nr02278j.

[36] M.G.A. El-Wahed, M.S. Refat, S.M. El-Megharbel, Synthesis, spectroscopic and thermal characterization of some transition metal complexes of folic acid, Spectrochim. Acta A 70 (4) (2008) 916–922.

[37] S. Ullah, A.K. Azad, A. Nawaz, K.U. Shah, M. Iqbal, G.M. Albadrani, F.A. Al-Joufi, A.A. Sayed, M.M. Abdel-Daim, 5-fluorouracil-loaded folic-acid-fabricated chitosan nanoparticles for site-targeted drug delivery cargo, Polymers (Basel) 14 (10) (2022 May 13) 2010, https://doi.org/10.3390/polym14102010.

[38] G. Nwanisobi, P. Ukoha, Spectrophotometric determination of niacin using 2,3-dichloro-5,6-dicyano-1,4-benzoquinone, Asian J. Chem. 28 (11) (2016) 2371–2374.

[39] Essa, M.L., Aya A. Elashkar, Hanafy, N.A.N., Ebrahem Saied, E.M., El-Kemary, M.A Dual targeting nanoparticles based on hyaluronic and folic acids as a promising delivery system of the encapsulated 4-Methylumbelliferone (4-MU) against invasiveness of lung cancer in vivo and in vitro.

[40] A. Alemi, J. Zavar Reza, F. Haghiralsadat, H. Zarei Jaliani, M. Haghi Karamallah, S.A. Hosseini, Karamallah S. Haghi, Paclitaxel and curcumin coadministration in novel cationic PEGylated niosomal formulations exhibit enhanced synergistic antitumor efficacy, J. Nanobiotechnol. 16 (1) (2018 Mar 23) 28, https://doi.org/10.1186/s12951-018-0351-4.

[41] M.P. Vinardell, H. Llanas, L. Marics, M. Mitjans, In vitro comparative skin irritation induced by nano and non-nano zinc oxide, Nanomaterials (Basel) 7 (3) (2017 Mar 4) 56, https://doi.org/10.3390/nano7030056.

[42] L. Benov, Effect of growth media on the MTT colorimetric assay in bacteria, PLoS One 14 (8) (2019 Aug 27) e0219713, https://doi.org/10.1371/journal.pone.0219713.

[43] A. Adan, G. Alizada, Y. Kiraz, Y. Baran, A. Nalbant, Flow cytometry: basic principles and applications, Crit. Rev. Biotechnol. 37 (2) (2017 Mar) 163–176, https://doi.org/10.3109/07388551.2015.1128876.

[44] K.M. McKinnon, Flow cytometry: an overview, Curr. Protoc. Immunol. 120 (2018 Feb 21) 5.1.1–5.1.11, https://doi.org/10.1002/cpim.40.

[45] Claudia A. Benavente, Elaine L. Jacobson, Niacin restriction upregulates NADPH oxidase and reactive oxygen species (ROS) in human keratinocytes, Free Radic. Biol. Med. 44 (4) (2008) 527–537, https://doi.org/10.1016/j.freeradbiomed.2007.10.006.
[46] P.B. Araveti, A. Srivastava, Curcumin induced oxidative stress causes autophagy and apoptosis in bovine leucocytes transformed by Theileria annulata, Cell Death Discov. 5 (2019) 100, https://doi.org/10.1038/s41420-019-0180-8.
[47] S.W. Kim, J.H. Lee, J.H. Moon, U.M. Nazim, Y.J. Lee, J.W. Seol, J. Hur, S.K. Eo, J.H. Lee, S.Y. Park, Niacin alleviates TRAIL-mediated colon cancer cell death via autophagy flux activation, Oncotarget 7 (4) (2016) 4356–4368, https://doi.org/10.18632/oncotarget.5374.
[48] J.J. Collier, F. Suomi, M. Oláhová, T.G. McWilliams, R.W. Taylor, Emerging roles of ATG7 in human health and disease, EMBO Mol. Med. 13 (12) (2021 Dec 7) e14824, https://doi.org/10.15252/emmm.202114824.
[49] W. Guo, J. Liu, W. Li, H. Ma, Q. Gong, X. Kan, Y. Cao, J. Wang, S. Fu, Niacin alleviates dairy cow mastitis by regulating the GPR109A/AMPK/NRF2 signaling pathway, Int. J. Mol. Sci. 21 (9) (2020 May 8) 3321, https://doi.org/10.3390/ijms21093321.
[50] S. Vega-Rubín-de-Celis, The role of Beclin 1-dependent autophagy in cancer, Biology (Basel) 9 (1) (2019 Dec 22) 4, https://doi.org/10.3390/biology9010004.
[51] Qian, Hao-Ran et al. "Interplay between apoptosis and autophagy in colorectal cancer." Oncotarget vol. 8,37 62759–62768. 27 Jun. 2017, doi:10.18632/oncotarget.18663.
[52] B.B.S. Jaswal, V. Kumar, H.C. Swart, J. Sharma, P.K. Rai, V.K., Singh multi–spectroscopic analysis of cholesterol gallstone using TOF–SIMS, FTIR and UV–vis spectroscopy, Appl. Phys. B. 121 (2015) 49–56, https://doi.org/10.1007/s00340-015-6200-3.
[53] W.J. Liu, L. Ye, W.F. Huang, et al., p62 links the autophagy pathway and the ubiqutin–proteasome system upon ubiquitinated protein degradation, Cell Mol. Biol. Lett. 21 (2016) 29, https://doi.org/10.1186/s11658-016-0031-z.
[54] Q. Wu, M. Xiang, K. Wang, Z. Chen, L. Long, Y. Tao, Y. Liang, Y. Yan, Z. Xiao, S. Qiu, B. Yi, Overexpression of p62 induces autophagy and promotes proliferation, migration and invasion of nasopharyngeal carcinoma cells through promoting ERK signaling pathway, Curr. Cancer Drug Targets 20 (8) (2020) 624–637.
[55] J.Y. Park, H.Y. Sohn, Y.H. Koh, et al., Curcumin activates Nrf2 through PKCδ-mediated p62 phosphorylation at Ser351, Sci. Rep. 11 (2021) 8430, https://doi.org/10.1038/s41598-021-87225-8.
[56] K. Liu, P.C. Liu, R. Liu, X. Wu, Dual AO/EB staining to detect apoptosis in osteosarcoma cells compared with flow cytometry, Med. Sci. Monit. Basic Res. 21 (2015 Feb 9) 15–20, https://doi.org/10.12659/MSMBR.893327.
[57] K. Liu, P.C. Liu, R. Liu, X. Wu, Dual AO/EB staining to detect apoptosis in osteosarcoma cells compared with flow cytometry, Med. Sci. Monit. Basic Res. (21) (2015 Feb 9) 15–20, https://doi.org/10.12659/MSMBR.893327.
[58] M.M. Mabrouk Zayed, H.A. Sahyon, N.A.N. Hanafy, M.A. El-Kemary, The effect of encapsulated Apigenin nanoparticles on HePG-2 cells through regulation of P53, Pharmaceutics 14 (6) (2022 May 29) 1160 https://doi.org/10.3390/pharmaceutics14061160 (PMID: 35745733).
[59] J.M.M. Levy, C.G. Towers, A. Thorburn, Targeting autophagy in cancer, Nat. Rev. Cancer 17 (9) (2017 Sep) 528–542 https://doi.org/10.1038/nrc.2017.53 (Epub 2017 Jul 28. PMID: 28751651).
[60] S.W. Kim, J.H. Lee, J.H. Moon, U.M. Nazim, Y.J. Lee, J.W. Seol, J. Hur, S.K. Eo, J.H. Lee, S.Y. Park, Niacin alleviates TRAIL-mediated colon cancer cell death via autophagy flux activation, Oncotarget 7 (4) (2016 Jan 26) 4356–4368 https://doi.org/10.18632/oncotarget.5374 (PMID: 26517672; PMCID: PMC4826210).
[61] H. Sun, G. Li, W. Zhang, Q. Zhou, Y. Yu, Y. Shi, S. Offermanns, J. Lu, N. Zhou, Niacin activates the PI3K/Akt cascade via PKC- and EGFR-transactivation-dependent pathways through hydroxyl-carboxylic acid receptor 2, PLoS One 9 (2014) e112310.
[62] C. Cantó, K.J. Menzies, J., Auwerx NAD+ metabolism and the control of energy homeostasis: a balancing act between mitochondria and the nucleus, Cell Metab. 22 (2015) 31–53.
[63] S.Y. Jang, H.T. Kang, E.S. Hwang, Nicotinamide-induced mitophagy: event mediated by high NAD+/NADH ratio and SIRT1 protein activation, J. Biol. Chem. 287 (23) (2012 Jun 1) 19304–19314, https://doi.org/10.1074/jbc.M112.363747.
[64] N.A.N. Hanafy, S. Leporatti, M. El-Kemary, Mucoadhesive curcumin crosslinked carboxy methyl cellulose might increase inhibitory efficiency for liver cancer treatment, Mater. Sci. Eng. C Mater. Biol. Appl. 116 (2020 Nov) 111119, https://doi.org/10.1016/j.msec.2020.111119.
[65] Nemany A. Hanafy, Nano targeted therapies loaded by curcumin against liver and breast cancer, 6th Euroscicon Conference on Nanotechnology July 30, 2020, Online Event.
[66] W. Guo, W. Li, Y. Su, S. Liu, X. Kan, X. Ran, Y. Cao, S. Fu, J. Liu, GPR109A alleviate mastitis and enhances the blood milk barrier by activating AMPK/Nrf2 and autophagy, Int. J. Biol. Sci. 17 (15) (2021 Oct 17) 4271–4284, https://doi.org/10.7150/ijbs.62380.
[67] N. Deleyto-Seldas, A. Efeyan, The mTOR-autophagy axis and the control of metabolism, Front. Cell Dev. Biol. (9) (2021 Jul 1) 655731, https://doi.org/10.3389/fcell.2021.655731.
[68] S.W. Kim, J.H. Lee, J.H. Moon, U.M. Nazim, Y.J. Lee, J.W. Seol, J. Hur, S.K. Eo, J.H. Lee, S.Y. Park, Niacin alleviates TRAIL-mediated colon cancer cell death via autophagy flux activation, Oncotarget 7 (4) (2016 Jan 26) 4356–4368, https://doi.org/10.18632/oncotarget.
[69] J. Pan, C. Lu, W. Jun, Y. Wu, X. Shi, Y. Ding, The up-regulation of P62 levels is associated with resistance of sorafenib in hepatocarcinoma cells, Int. J. Clin. Exp. Pathol. 12 (7) (2019 Jul 1) 2622–2630 (PMID: 31934090).
[70] T. Jiang, B. Harder, M. Rojo de la Vega, P.K. Wong, E. Chapman, D.D. Zhang, p62 links autophagy and Nrf2 signaling, Free Radic. Biol. Med. 88 (Pt B) (2015 Nov) 199–204, https://doi.org/10.1016/j.freeradbiomed.
[71] Y. Chimura, S. Waguri, Y.S. Sou, S. Kageyama, J. Hasegawa, R. Ishimura, T. Saito, Y. Yang, T. Kouno, T. Fukutomi, T. Hoshii, A. Hirao, K. Takagi, T. Mizushima, H. Motohashi, M.S. Lee, T. Yoshimori, K. Tanaka, M. Yamamoto, M. Komatsu, Phosphorylation of p62 activates the Keap1-Nrf2 pathway during selective autophagy, Mol. Cell 51 (5) (2013 Sep 12) 618–631, https://doi.org/10.1016/j.molcel.2013.08.003.
[72] N.A.N. Hanafy, R.H. Abdelbadea, A.E. Abdelaziz, et al., Formulation and optimization of folate-bovine serum albumin-coated ethoniosomes of pterostilbene as a targeted drug delivery system for lung cancer: in vitro and in vivo demonstrations, Cancer Nano 14 (2023) 49, https://doi.org/10.1186/s12645-023-00197-4.
[73] N.A.N. Hanafy, Extracellular alkaline pH enhances migratory behaviors of hepatocellular carcinoma cells as a caution against the indiscriminate application of alkalinizing drug therapy: in vitro microscopic studies, Acta Histochem. 125 (4) (2023 May) 152032, https://doi.org/10.1016/j.acthis.2023.152032.
[74] Ghazy, M.G.M & Hanafy, N.A.N. Targeted therapies for breast and lung cancers by using propolis loaded albumin protein nanoparticles. Scientific Reports 2023 (Under review).